nature nanotechnology

SUPPLEMENTARY INFORMATION

DOI: 10.1038/NNANO.2009.220

Placement and orientation of individual DNA shapes on lithographically patterned surfaces

Supplementary Materials

Ryan J. Kershner[†,1] Luisa D. Bozano[†] Christine M. Micheel[†,2]
Albert M. Hung[†,3] Ann R. Fornof[†,4] Jennifer N. Cha[†,3]
Charles T. Rettner[†] Marco Bersani[†,5] Jane Frommer[†]
Paul W. K. Rothemund[§,*] Greg M. Wallraff[†,*]

1 Origami preparation and purification

Triangular DNA origami were self-assembled according to Rothemund ("sharp triangles** with bridges", [4]) using a one-pot synthesis in a standard thermal cycler (Applied Biosystems Geneamp PCR System 9700). DNA oligonucleotides (staples) were obtained unpurified from IDT DNA Technologies (Coralville, IA), single-stranded m13mp18 phage DNA (M13) was obtained from NEB (Ipswich, MA). Generally, about four 50 μL tubes of DNA origami were made at a time, and each batch would include origami for multiple experiments. In each 50 μL PCR tube, 5 μL 10$\times$ TAE buffer (400 mM Tris acetate, 10 mM EDTA, 20 mM Na^+) with 125 mM $MgCl_2$ (to make 12.5 mM $MgCl_2$ in the 1X solution) was mixed with 5 μL of $\sim$10 nM single-stranded circular M13 DNA, enough staple solution to make 100 nM of each staple in 50 μL final volume, and enough distilled H_2O to make 50 μL total solution per tube. The program used to anneal the DNA in the thermal cycler was as follows: 1) heat to 90°C and hold for 5 minutes, 2) cool at the slowest ramp rate to 20°C, 3) repeat steps one and two, and 4) cool to 4°C and hold until sample retrieval. Step three is not necessary for high-quality origami formation; it was present due to programming restrictions of our particular thermal cycler. After completion of the thermal cycling step, excess staples were removed from the origami solutions by washing at least 3 times with 250–400 μl of 1$\times$ TAE/Mg^{2+} buffer in 100 kDa MWCO centrifuge filters (Microcon YM-100, Millipore, Billerica, MA). Filters were centrifuged on a single-speed benchtop microcentrifuge (VWR Galaxy Ministar) at $\sim$2000 g for 30–90 seconds. Care must be taken not to centrifuge the filter to dryness, as the origami will stick to the filter, resulting in significant loss of sample; instead centrifuge until 25–50 μl of the sample is left. After filtration the origami solutions were stored at 4°C until use. We found that this filtration step was important in achieving high populations of adsorbed origami on the templates. Experiments with unfiltered solutions had lower yields of bound origami, possibly due to competition with high concentrations of oligonucleotide staples for the template binding sites.

[†]Almaden Research Center, San Jose, CA 95120, USA. Present address: [1]University of Wisconsin, Madison, WI 53706, USA. [2]The National Academies, Washington, DC 20001, USA. [3]Dept. of Nanoengineering, University of California, San Diego, CA 92093, USA. [4]Center for Nanoscience, Ludwig-Maximilians Universität, 80799 Munich, Germany. [5]Dipartimento di Fisica, Università di Padova, I-35131 Padova, Italy.

[§]Depts. of Bioengineering, Computer Science, and Computation & Neural Systems, California Institute of Technology, Pasadena, CA 91125, USA.

*Corresponding authors. email: pwkr@dna.caltech.edu and gmwall@almaden.ibm.com.

**DNA origami can aggregate via π-π interactions between the ends of the DNA helices that comprise them. It is important to use a non-aggregating DNA origami in positioning studies such as this one. The sharp triangle, which has all of the ends of its DNA helices hidden within the structure, is a non-aggregating origami. However, other DNA origami, such as the rectangle designs from ref. 4, can be rendered non-aggregating by omitting the DNA strands along the edges of the DNA origami. The rectangles could then be used in positioning studies.

DOI: 10.1038/NNANO.2009.220

2 Lithographic Patterning

E-beam Lithography E-beam samples were prepared on a Leica VB6 100KeV Gaussian beam tool. Two levels of lithography were used for template fabrication. Substrates were first patterned using 10 μm-size alignment marks employing a gold liftoff process. A second e-beam exposure was used to pattern the origami binding sites. The alignment marks were used both (1) to find the patterned region when templates were cleaved from substrates and (2) to position the patterned region in the microscope prior to AFM imaging.

The gold alignment marks were patterned as follows: A 500 nm thick film of poly methylmethacrylate (PMMA, MicroChem Corp., Newton, MA) with molecular weight 950,000 diluted 5% in Anisole was spun-cast onto a 125 mm silicon substrate wafer and soft-baked for 15 min at 175°C. Following e-beam exposure the sample was developed for 2 minutes in a 1:3 mixture of methylisobutyl ketone:isopropyl alcohol (MIBK:IPA), rinsed with IPA and dried then with a stream of nitrogen. The patterned resist film was then coated with a 10 nm film of a chromium adhesion layer followed by a 50 nm thick film of gold at a deposition rate of 20 Å/sec. The metal-coated resist film was removed from the substrate by soaking the wafer in a sonicated N-methylpyrrolidone (NMP) bath for 30 min followed by IPA and water rinses leaving behind the desired pattern of metal lines. These alignment marks were patterned on top of the carbon film in the case of the DLC templates and on the oxide surface for the TMS/SiO_2 templates.

The substrate was then coated with a 100 nm film of the PMMA photoresist, exposed and developed as described above. Aligned patterns with feature sizes ranging from 90 to 400 nm consisting of arrays of lines and shapes such as triangles, rectangles and hexagons were fabricated with exposure doses between 800 and 1100 μC/cm^2 depending on the sizes and shape of the printed features.

The sharpness of features at corners (say, the degree of rounding of the corners of triangles), fidelity to the desired size (whether features in the mask turn out to match the size of the e-beam pattern), and the completeness of resist removal during development were strongly dependent on exposure dose. To verify that shapes were well-formed, correctly sized, and that little or no resist was present in the bottom of features in the resist layer (after exposure and developing), we employed a lift-of procedure to generate Au/Cr replicas of the features. 5 nm of a chromium adhesion layer followed by 10 nm of a gold contrast layer were evaporated onto a patterned resist film, the resist was stripped, and the resulting metal features were imaged by SEM. An electron micrograph of a representative patterned resist film is shown in Figure 2b, inset. If any resist remained in resist features after development then the metal did not adhere during liftoff, indicating that exposure dose should be increased.

Optical Imaging Optical lithography (193 nm) was done in a single step with an ISI ArF microstepper with an NA of 0.6 (10× reduction ratio) employing a binary chrome-on-quartz mask and a field size of 4×4 mm. Due to the relatively large field size, alignment marks were not required. Patterned arrays of lines and vias (holes) were generated in a positive tone ArF photoresist (JSR 1682). The resist was cast on the 125 mm substrate as a 150 nm film, soft-baked at 120°C for 90 sec, exposed, and then baked for 60 sec at 110°C. The imaged resist film was developed for 60 seconds (single puddle) in a solution of 0.26 N tetramethylammonium hydroxide (TMAH, Air Products Optiyield CD).

3 Template Fabrication

TMS/SiO_2 templates The TMS/SiO_2 templates were fabricated on thermal SiO_2 surfaces on silicon substrates. All experiments were performed on wafers coated with a 1 micron film of thermal oxide. Bare wafers were used for optical lithography, wafers pre-patterned with alignment marks were employed for e-beam imaging. The wafers were cleaned by treatment with UV-ozone for 30 minutes (JELIGHT UVO Cleaner Model 342) at room temperature to give an oxide surface with a water contact angle of $< 10^\circ$ (static angle as measured on VCA XE 2500 instrument). The clean wafers were immediately transferred to a Genesis priming oven and hexamethyldisilazane (HMDS) was vapor deposited for 60 s at an oven temperature of $150^\circ C$ using standard protocols. After silylation the water contact angle of the freshly treated surface of thermal oxide was 60–70°. The wafer was then coated with photoresist, exposed, and developed as described above. In the case of large optical features, UV-ozone treatment for 5 min was sufficient to remove the trimethylsilyl (TMS) functionality from the patterned areas and expose a hydrophilic surface. For the smaller e-beam features, a short isotropic etch of 7 seconds in an oxygen plasma (PX 250 March Plasma Systems) was found to give the best results (Etch 1 data, in Fig. 1c,d,g and repeated in Fig. S1,S2, and S20a). An alternative O_2 plasma etch (using a Surface Technology System MultiPlex Inductively Coupled Parallel plate plasma etch tool under conditions of low power, low bias and low pressure), an anisotropic etch of 3 seconds, gave similar quality orientation, but many more double binding events (in which two origami bound to a single patterned triangle) were observed (Etch 2 data, Fig. S3,S4, and S20b).

After dry oxidative etching, the photoresist was stripped from the substrate to yield a patterned template consisting of an array of hydrophilic regions on a hydrophobic surface. This last step proved to be the most sensitive step in this process since it is necessary to completely remove the photoresist while leaving intact the organic surface layer in the unexposed regions of the template. Our initial stripping attempts employed mild room temperature procedures with solvents such as acetone and dichloromethane. Unfortunately these procedures left contaminated surfaces even in the patterned areas that had been UV-ozone treated (contact angles of 25-40°). No origami binding was observed and considerable debris was seen on the surface. Switching to a more aggressive strip procedure employing sonicated NMP at a temperature $55^\circ C$ for 22 min produced functional templates. The contact angle for the hydrophilic regions of the templates were $< 10^\circ$ with that of the unpatterned template surface retaining a value of $\geq 40^\circ$. Good selectivity of origami binding was observed on templates prepared using this procedure. The same resist-stripping procedure was used for both optical and e-beam patterned wafers.

Hydrolytic instability of TMS monolayers was monitored by changes in contact angle. In one experiment freshly HMDS-primed SiO_2 had a contact angle of 66.1°. After ~2 hours under 10× TAE buffer with 125 mM $MgCl_2$ the contact angle decreased to 40.7°. After a total of 17 hours under buffer the contact angle dropped to 33.9°. How this change affects the effectiveness of the TMS monolayer as a non-binding background for DNA origami has not been examined.

DLC/DLC templates 125 mm silicon wafers were sputter cleaned for 30 sec. and diamond-like carbon was deposited employing a methane plasma in a manner similar to that described in [28]. To enhance adhesion, 0.3 nm of silicon was deposited prior to the DLC layer. The DLC films were deposited at normal incidence, using a VEECO IBD system run with a 210 mm low power grid, which extracts ions from the methane plasma. The resulting 10 nm thick films have an estimated carbon sp^3/sp^2 hybridization ratio of 3 to 4 with a hydrogen content in the range 30-32%. The films as deposited have a water contact angle of 64°.

DOI: 10.1038/NNANO.2009.220

The wafer was first patterned with alignment marks and then patterned with the desired template features as described above. A relief pattern was etched into the DLC surface using the oxygen plasma asher listed above. A minimum etch time of 5 seconds was required to strike the plasma and yielded a DLC etch depth of approximately 0.5 nm as measured by AFM. An etch time of 12 seconds gave a corresponding feature depth of 1.2 nm to 1.4 nm. The rate was found to be linear up to 20 or more seconds, after which time the PMMA was generally completely removed and further selective patterning could not be achieved. As for the TMS/SiO_2 system, complete removal of the photoresist after etch was critical in achieving selective origami deposition and an aggressive resist stripping procedure was employed to clean the DLC templates. The substrates were first cleaned in a freshly prepared piranha bath (3:1 mixture of sulfuric acid with 30% hydrogen peroxide) for 30 minutes, and then thoroughly rinsed in deionized water (DI). This was immediately followed by immersion in a sonicated bath of a commercial resist stripper (JT Baker ALEG-310) at 55°C for 30 minutes, a thorough DI rinse and nitrogen blow dry. Two identical passes of these steps seemed to give the best results. We note that this procedure gave very clean surfaces, but because the piranha treatment is a wet chemical oxidative etch which oxidized the background as well, the procedure confounded surface analysis of the DNA origami binding features (see next subsection). It is possible that an aggressive NMP stripping procedure might yield similar binding and orientation results while leaving the background unoxidized and hydrophobic.

The DLC background, while oxidized and made wettable by the piranha treatment, is fairly stable given further piranha treatments. This allows one path to re-use: after aligning origami on a DLC/DLC patterned substrate, the pattern can be piranha treated, rinsed and reused. Substrates treated in this way could be reused 4-5 times before the selectivity between the background and features is noticably reduced and origami adsorb everywhere. Figs. S9 and S10 show the results of a second use of the substrate used in Fig. 1f, S7 and S8. Fig. S20 shows the angular dispersion before (c) and after (d) piranha treatment. Because we cannot yet distinguish the background and features with respect to the amount of oxygen-bound carbon species, we hypothesize that subsequent piranha treatments are changing the type of oxidized carbon species. Also we note that less harsh cleaning steps (mere detergents, weak acid, or weak base) might allow reuse of DLC/DLC substrates and should be tried.

Surface characterization of DLC As noted above, the piranha clean process used as part of the resist strip resulted in a completely hydrophilic surface as measured for films of both the unetched and plasma-etched DLC films. (Hydrophilicity is clearly not sufficient for DNA binding in these systems.) To better understand the origami adsorption process, the DLC surface chemistry was characterized by X-ray photoelectron spectroscopy (XPS). A Physical Electronics Quantum 2000 ESCA Microprobe with a monochromatic Al K_α source was used in these experiments. DLC samples receiving different treatments were analyzed and surface atomic percent compositions, C_i, were calculated as follows:

$$C_i = \frac{\frac{I_i}{\sigma_i}}{\sum_{\text{all } k} \frac{I_k}{\sigma_k}} \tag{1}$$

where, for k peaks, the (I_i/σ_i) are the peak areas I_i of the kinetic energy, corrected for elemental photoionization cross-sections, σ_i. Uniform lateral and depth distributions were assumed. These results, along with water contact angles measured with a Data Physics OCA instrument, for the different surfaces are shown in the table below. The oxygen/carbon peak ratio is shown for clarity. Other elements (*) include N 1s, Si 2p, S 2p, F 1s, Na 1s. The takeoff angle was 10°.

surface treatment	contact angle	carbon 1s (C1s)	oxygen 1s (O1s)	Other*	O 1s/C 1s
untreated DLC	64°	85.3 ± 0.3%	14.7 ± 0.2%	0	0.17
ALEG resist strip treatment	44°	81.4 ± 0.5%	14.9 ± 0%	3.6 ± 0.9%	0.18
piranha-cleaned	< 10°	76.2 ± 0.5%	23.1 ± 0.5%	0.8 ± 0.1%	0.30
12 sec O_2 plasma etched	< 10°	74.7 ± 1.9%	25.1 ± 1.9%	0.2 ± 0%	0.34

The results reveal a significant increase in the surface oxygen content for the hydrophilic plasma-etched and piranha-cleaned DLC as compared with the pristine (untreated) surface. No change in the surface composition of the surface treated only with resist stripper (ALEG-310) was detected. XPS data taken at higher takeoff angles (45° and 85°) show that the oxygenation is confined to the surface with virtually no other peaks detected in the bulk aside from the carbon 1s (C 1s). These data are consistent with the observation that origami do not adhere to an untreated hydrophobic DLC surface but do not explain the high selectivity observed between the two hydrophilic surfaces: DNA structures bind strongly to the plasma-etched surfaces but not to the chemically-oxidized surface of the piranha-cleaned samples.

Further, comparison of individual C 1s spectra for piranha treatment and the total treatment experienced by features (piranha + ALEG + O_2 plasma), show similar increases in higher oxidation state species (via a peak at 288 eV) again failing to distinguish between piranha-treated surfaces and surfaces treated as features. The spectra for O_2 plasma treatment alone gave, suprprisingly, a 40% higher peak at 288 eV than plasma treatment in combination with the other treatments (piranha + ALEG + O_2 plasma) but the significance of this is unclear.

A peak in the C 1s XPS spectra at 288 eV is indicative of high oxidation state carbon in the surface—carbonyls, carboxylates, etc. Initial attempts to confirm this via single reflection ATR FT-IR spectroscopy have so far failed to detect carbonyl absorbances. We do not put weight on this negative result, more careful characterization by FT-IR is merited and further surface studies of the DLC/DLC system will be needed to elucidate binding mechanism and to determine whether and how O_2 plasma treatment facilitates charge inversion in the presence of 100 mM $MgCl_2$.

DOI: 10.1038/NNANO.2009.220

4 AFM Imaging

Sample preparation Samples for AFM imaging were prepared as follows: 5-6 mm square template fragments were cleaved from the patterned substrates and mounted in the AFM liquid imaging cell. 1-5 μL of the filtered origami solution plus 20-45 μL of additional buffer at the desired $MgCl_2$ concentration was pipetted onto the surface such that the percentage of origami formation solution in the imaging buffer was 5-10%. Due to uncertainties about the initial yield of origami and losses incurred during filtration the actual concentration of origami in contact with the template is unclear but is certainly less than the 1 nM concentration of the M13 virus. For the DLC/DLC templates (the first system we explored) the origami formation solution and binding buffer were placed on the surface and imaging was begun within several minutes. For trimethylsilyl/silicon dioxide (TMS/SiO_2) templates, better results were obtained if origami were allowed to adsorb for 2 to 3 hrs before the sample was imaged. During this incubation period the wet sample was stored in a closed container ringed with a moistened Kimwipe to minimize evaporation. The longer incubation times may partially explain the relatively denser coverage of origami on line features on TMS/SiO_2 (e.g. compare Fig. 1c to Fig 1e). Future DLC/DLC experiments might thus benefit from longer incubation times, however it is possible that differences in coverage might be explained by differences in binding affinity or binding kinetics for the two surfaces.

$MgCl_2$ and buffer concentrations All origami were formed in 12.5 mM $MgCl_2$ / 1× TAE buffer (40 mM Tris acetate, 1 mM EDTA, 2 mM Na^+). The divalent cation Mg^{2+} screens the DNA backbone repulsion, allowing the DNA to self-assemble and stabilizes the branched junctions of the origami; Tris serves as the monovalent cation in the TAE buffer. Unless otherwise noted origami were bound to patterned substrates in 100–125 mM $MgCl_2$ / 9–10× TAE buffer; in the binding buffer Mg^{2+} appears to serve to invert the charge of the features and allow negatively-charged DNA origami to bind.

Facts to note up front are that (A) it is unusual to use TAE buffers as buffers in biochemistry or biophysical experiments—Tris buffers are usually avoided because of their temperature dependent pH—and (B) it is even more unusual to use TAE buffers at such high strength (10×, 400 mM Tris) as we do here. (A) is a relic, a legacy procedure from the field of DNA nanotechnology whose practitioners uses TAE/Mg^{2+} buffers in the gel electrophoresis of DNA nanostructures and continue to do so in imaging and biophysical experiments to keep conditions exactly the same. (B) is an artifact of experimental convenience: the stock solution (10× TAE, 125 mM $MgCl_2$) used in the preparation of 1× TAE, 12.5 mM $MgCl_2$ formation buffer for the DNA origami was readily at hand for these experiments. Another potentially confusing feature of TAE buffers is that the EDTA they contain chelates Mg^{2+}. Thus the amount of free Mg^{2+} available for binding the DNA to the surface is reduced by the amount of EDTA in solution. The purpose of the EDTA is to chelate other contaminant ions that might degrade the DNA; 1 mM is suitable for this purpose and so it is unusual to use such high, 10 mM concentrations of EDTA. But here, the relative concentrations of EDTA and $MgCl_2$ are always such that the amount of free $MgCl_2$ is reduced by no more than 8%.

While we have not exhaustively examined the phase diagram of origami/feature binding as a function of Mg^{2+} and the concentration of Tris, we have observed a few trends. The following tables report our experiments with varying $MgCl_2$ and TAE concentrations on TMS/SiO_2 and DLC/DLC.

For the TMS/SiO_2 system we found:

$MgCl_2$	1× TAE	9.1–10× TAE
12.5 mM	no binding*	no binding
100–125 mM	binding*	binding†
1 M	low binding*	—

For DLC/DLC we found:

$MgCl_2$	1× TAE	5.5 × TAE	9.1–10× TAE
12.5 mM	no binding	—	no binding
69 mM	—	no binding*	—
100–125 mM	—	—	binding*,†
1 M	—	—	low binding*

('—' indicates an untried condition, '*' a condition reported in Fig. 29, '†' condition under which most data was taken.) Things to note:

1. $\sim$ 100 mM Mg2+ is necessary for binding on SiO_2 features, and sufficient for binding regardless of the buffer strength (1× or 10× TAE).

2. 1 M mM Mg^{2+} greatly decreased binding on SiO_2 features in combination with 1× TAE, see Fig. S29f.

3. $\sim$ 100 mM Mg2+ was sufficient for binding on DLC features in combination with 10× TAE.

4. $\sim$ 70 mM Mg^{2+} was *not* sufficient for binding on DLC features in combination with 5.5× TAE, see Fig. S13 suggesting that charge inversion occurs between 70 mM and 100 mM Mg^{2+}.

5. 1 M mM Mg^{2+} greatly decreased binding on DLC features in combination with 10× TAE, see Fig. S14 and S15.

While we have not tested 1× TAE with $\sim$ 100 mM Mg^{2+} on DLC features, it is likely that binding would be observed. The use of TAE buffers here is probably of no great importance—its use in AFM of DNA nanostructures should not be fetished or fossilized and, in reproducing this work an experimenter should have no compunction about decreasing the TAE strength or changing buffer—note that the high pH (8.3) may play a role in the Mg^{2+} concentration at which binding is observed, we have not yet explored the effect of pH but ref. 31 suggests that at pH 7.5 at least 350 mM Mg^{2+} would be required for binding on SiO_2.

In fact it is likely that TAE concentration acts antagonistically with Mg^{2+} and actually increases the concentration of Mg^{2+} required for binding. Monovalent cations have this effect for DNA binding on mica, as laid out in great detail in a DNA binding phase diagram for Mg^{2+} in combination with Na^+ in ref. 29. The concentration at which monovalent cation (in ref. 29, Na^+) prevents binding to mica increases with the concentration of Mg^{2+}. That is, Mg^{2+} compensates for the presense of monovalent cation until its own (constant) threshhold for causing dissociation is reached (1 M)—this is likely the concentration at which DNA becomes overcharged (positively charged) and no longer binds the surface. Thus our observation that 1 M $MgCl_2$ inhibits DNA binding for both systems is also consistent with ref. 29's phase diagram.

Finally, it is likely that multivalent cations other than Mg2+ will serve to bind DNA to features in positioning experiments. Ni^{2+}, Zn^{2+}, and Co^{3+} all bind DNA to mica *more readily* (at lower concentrations) than does Mg2+ (H. Hansma & D. Laney, Biophysical Journal, **70**:1933–1939, 1996) and should be tried if convenient for other reasons.

DOI: 10.1038/NNANO.2009.220

Imaging under buffer AFM imaging was done in tapping mode in solution using an Asylum Research MFP-3D. NP-S oxide-sharpened silicon nitride probes (NP-S, Veeco Probes) were used for imaging, specifically tip C with a nominal stiffness of 0.32 N/m and frequencies of 56 kHz in air and 16 kHz in aqueous solution. Tip sharpness and substrate roughness were the primary factors limiting image resolution. The AFM tip was mounted in the commercially available liquid cell holder with a drop of buffer wetting the back side of the cantilever before being immersed and brought into contact with the sample surface. During imaging care was taken to minimize damage to the origami structures by reducing the drive amplitude and adjusting the amplitude set point in order to impart the lowest force possible.

Height images are typically presented for DLC/DLC samples but phase images are presented for TMS/SiO_2 samples because the topographic difference between unexposed TMS and the binding sites is too small to be easily observed. In some cases (e.g. for line features in Fig. 1e) we present phase images for DLC for purposes of clarity. The grayscale in the phase images we present has been inverted (from the way that it is usually presented, with negative phase being black) so that the origami present as white rather than black, to match the way that they appear in height images.

Sizes given for triangular sticky features are approximate for two reasons: (1) by AFM the size of sticky patches varies at least 10% within a single e-beam patterned area and (2) the triangles are not perfect triangles (the e-beam yields features with rounded corners) and so it is not clear what the best way to align a reference triangle on top of features. Here we scale reference triangles so that their edges aligned to the edges of triangles, rather than aligning their corners to the corners of triangles. This results in larger measurements for triangles. Better measurement of triangular feature size that incorporates a model of the feature shape may be requred to make accurate measurements of alignment as a function of feature size.

5 Characterization of binding and alignment

DNA nanostructures with the shape of equilateral triangles were selected for these studies because they are rigid, non-aggregating, and have a large, well-defined triangular hole in the center. Based on the edge length of the triangles in nucleotides (374 bases) and length of B-DNA (0.34 nm/base) the triangles have a theoretical size of 127 nm which is consistent with that obtained from well-calibrated AFM imaging. The hole is 160 bases/54 nm and aids in finding triangle orientation.

We examined our method's ability to position and align DNA origami triangles by measuring the number of occupied sites as well as the angle of the DNA origami with respect to those sites. Because AFM imaging is destructive and highly sensitive to imaging parameters, images of DNA origami triangles stuck to binding sites are sometimes incomplete or distorted. Hence it is difficult to know exactly when to count a site as occupied, or to measure an origami's orientation. Because the measurements and choices made have a subjective component, we include all data and annotations recording occupancy and alignment (Figs. S1–S19) so that a reader can decide for themselves whether the distributions we report (Fig. S20 and S21) reflect the image data. In analyzing the data, we observed that the number of cases in which we were uncomfortable making a classification (when data were on the edge of a just noticeable difference between classes in our classification scheme) were few and would not significantly alter our conclusions. Angles were measured with a resolution of 2.5° by fitting one of 48 pre-rotated triangles on top of each DNA triangle in the image. (A triangle was left unmeasured when there was more than one way to fit it.) These data were used to compute the peak positions and standard deviation; to create histograms 2.5° bins were combined into 5° bins (and plotted midway between the pairs of combined 2.5° bins).

The orientation data was taken from -60° to 57.5°, spanning a 120°range for which, because of the 3-fold symmetry of the triangles, $-60° \equiv +60°$. The periodic nature of the data means that one cannot find peaks by merely averaging the angles over any particlar range. For exmple, if a peak is centered at -60° (60°), and the range is -60° to 57.5°, approximately half of the area of the peak will fall in the positive half of the range and approximately half of the area will fall in the negative half; taking the average of the angles will give an answer of approximately 0°, clearly not the desired result. Our approach is to instead consider a sliding window, of 120° in width, and consider 48 possible offsets that give the 48 possible different cyclic permutations of the histogram. For each offset, we calculate the standard deviation of the collection of angles. We find the offset with minimum standard deviation, and we calculate the mean for that window/offset; we report the mean (adjusted by phase shift of the permutation and by adding or subtracting 120° until it is in the range -60 to 57.5) as the position of the peak and the standard deviation of the window as the standard deviation of the peak. To make this clear, our procedure was:

- Measure the alignment of N triangles, $-60° \leq \theta_{i,0} \leq 57.5°$ in increments of 2.5°, $i \in \{1..N\}$.
- For 47 new windows k, $k \in \{1..47\}$ let a permutation $\theta_{i,k} = \theta_{i,k-1} + 2.5$ if $\theta_{i,k-1} + 2.5 \leq 57.5$, otherwise $\theta_{i,k} = -60$.
- For each window $k \in \{0..47\}$, compute the mean $\Theta_k = \sum_{i=1}^{n} \theta_{i,k}/N$ and standard deviation $\sigma_k = \sqrt{\frac{1}{N-1}\sum_{i=1}^{n}(\theta_{i,k} - \Theta_k)^2}$.
- Report $\Theta_m - 2.5m$ adjusted to fall on [-60,57.5] as the peak position, and σ_m as its standard deviation for m such that $\sigma_m = \min_{k=0}^{47} \sigma_k$.

The m are not unique for our data, but for our data (on triangular features with 100 mM Mg^{2+}) minima in the standard deviation occur in continous runs of adjacent windows k so that Θ_m and σ_m are unique. See plots (green histograms) of the standard deviation as a function of the phase of the sliding window

DOI: 10.1038/NNANO.2009.220

in Fig. S20. These show that there are unique global minimum "plateaus" in our data for triangles on oriented binding sites (consistent with the hypothesis that our data represent single peaks).

The data on triangular features with 1 M Mg^{2+} (Fig. 21d) show no definite peak, although there are identifiable plateaus in the standard deviations for these data. These data are consistent with being drawn from distributions of randomly oriented triangles (see below). In addition to calculating the angular dispersion for triangular binding sites, we show angular dispersion analysis for DNA origami triangles on 350 nm, 200 nm and 500 nm line features (Fig. 21a,b,c) on TMS/SiO_2 and DLC/DLC. These data show no strong peaks associated with the edges of the line features. The 200 nm and 500 nm data happen to have single minima in their standard deviations, but the 350 nm data does not. For the 350 nm data we use the minima that has the lowest standard deviation to characterize the distribution. Samples of random angles often have single minima in similar histograms of their standard deviations, but often they do not.

The standard deviation of these angles is not a familiar measure and so it is natural to ask what the expected angular dispersion is for a sample of random angles. To get a feel for what the standard deviation for samples of random angles would look like, we averaged the angular dispersion (standard deviation) of 10^5 samples each with N random angles for all the different numbers of measurements N used in this paper. We also calculated the standard deviation of these average angular dispersions. This allowed us to calculate the p-value for each experimentally-measured angular dispersion of origami in the paper, the probability that a random distribution would have an angular dispersion equal to or less than that of the observed distribution. Average standard deviations ($\overline{\text{s.d.}}$) for 10^5 computer generated distributions, standard deviations of the average standard deviations ($\text{s.d.}''$), experimental standard deviations (s.d.), and p-values (p, rounded up to the nearest power of 10) are summarized here (some experiments had the same N):

N	15	15	40	40	43	44	68	71	94	96	112	132	148	203	240
$\overline{\text{s.d.}}$	29.8	29.8	31.5	31.5	31.6	31.6	32.2	32.2	32.5	32.5	32.7	32.8	32.9	33.1	33.2
$\text{s.d.}''$	2.8	2.8	1.6	1.6	1.6	1.5	1.2	1.2	1.0	1.0	.95	.88	.83	.71	.66
s.d.	32.0	29.2	21.6	21.1	20.4	22.3	30.7	17.5	13.1	12.0	13.3	8.4	12.5	32.0	33.3
p	.22	0.42	10^{-9}	10^{-10}	10^{-12}	10^{-9}	0.11	10^{-34}	10^{-77}	10^{-87}	10^{-91}	10^{-170}	10^{-132}	0.059	0.45

Under conditions of good binding (~100 mM Mg^{2+}), p-values ranged from 5×10^{-10} in the case of the down-oriented triangles in Fig. 20b down to 4×10^{-171} in the case of down-oriented triangles in Fig. 20c. It is not particularly surprising that the observed distributions for origami are easily statistically distinguished from random orientations, but given that the expected standard deviations and their standard deviations were not obvious *a priori*, it was important consider them. (Note for fun and completeness: in the limit of an infinite number of samples $N\rightarrow\infty$, for angles on [-60 57.5] discretized into 2.5° bins, $\overline{\text{s.d.}}=34.6°$.) For origami binding on DLC/DLC under 1 M Mg^{2+} the observed distributions of up and down-oriented triangles (Fig. S21d) are consistent with a distribution of randomly-oriented triangles ($p_{\triangle}=0.42$, $p_{\triangledown}=0.22$). (Where appropriate we calculated p-values based on the probability of the angular dispersion being greater than or equal to the observed value, as was the case for $p_{\triangledown}$).

We also used $\overline{\text{s.d.}}$ of computer-generated distributions to ask whether experimental data for line features are consistent with the hypothesis that trianglesthe line features are randomly-oriented. Here the p-values for 350 nm lines (0.45, Fig. S21a), 200 nm lines (0.11, Fig. S21b) and 500 nm lines (0.059, Fig. S21c) are large enough that we judge the orientations of triangles in these experiments to be random.

Significant offsets in orientation (from that desired) were observed for one of the TMS/SiO_2 samples, and all of the DLC/DLC samples. The offsets may be an artifact of tip/sample interaction under buffer—the AFM may be exerting an asymmetric force on the triangles, especially if the substrate is tilted. The offsets might also be attributed to a subtle, undetected asymmetry of the binding sites; qualitatively it seems the effect may be greater for sites having a greater size mismatch with the origami.

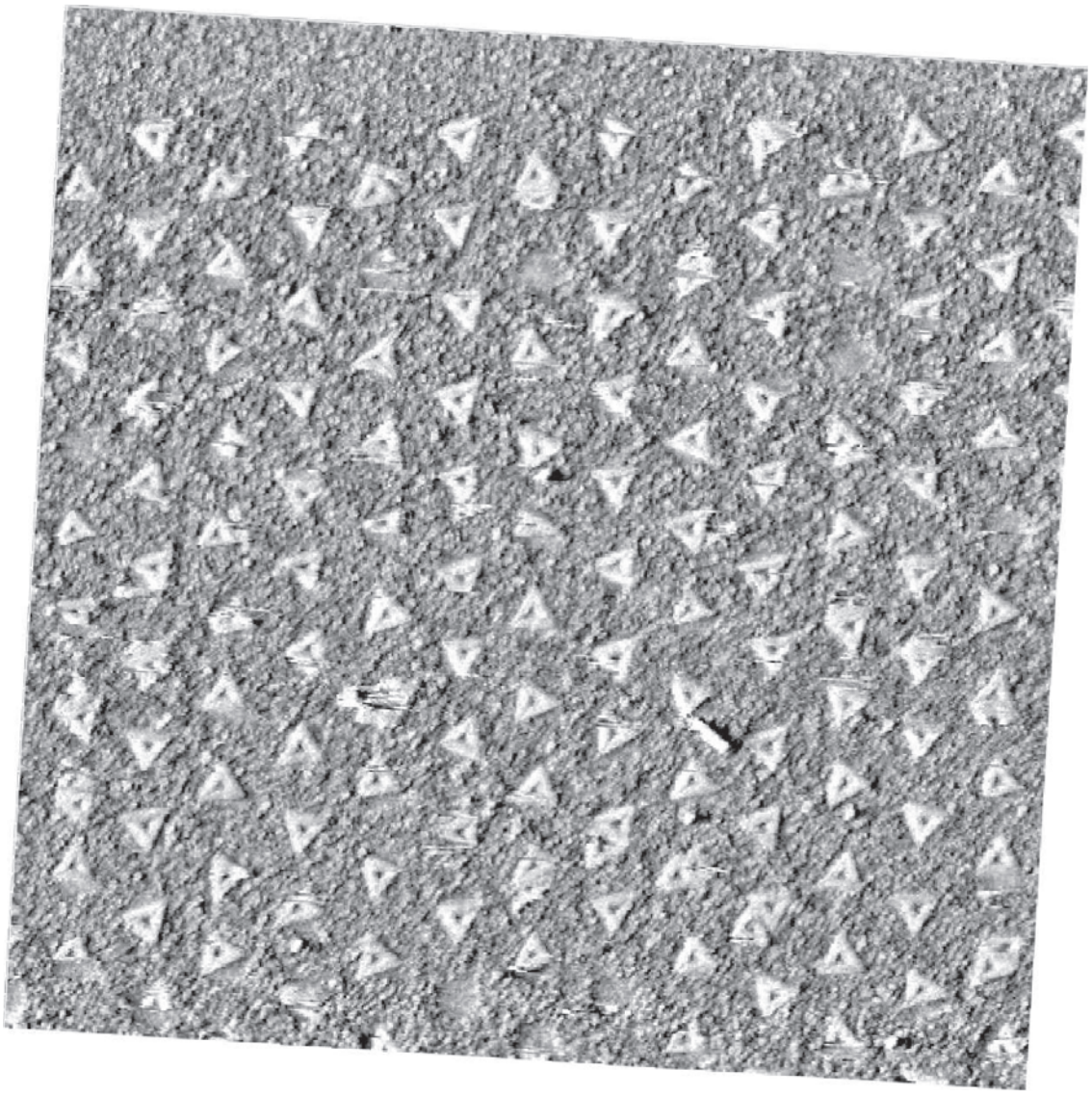

Figure S1: **DNA triangles on triangles patterned on a TMS/SiO_2 surface; etch condition 1. 125 mM $MgCl_2$/10×TAE** Unannotated 3 micron phase image. Phase runs from -2.5° (white) to 2.5° (black).

DOI: 10.1038/NNANO.2009.220

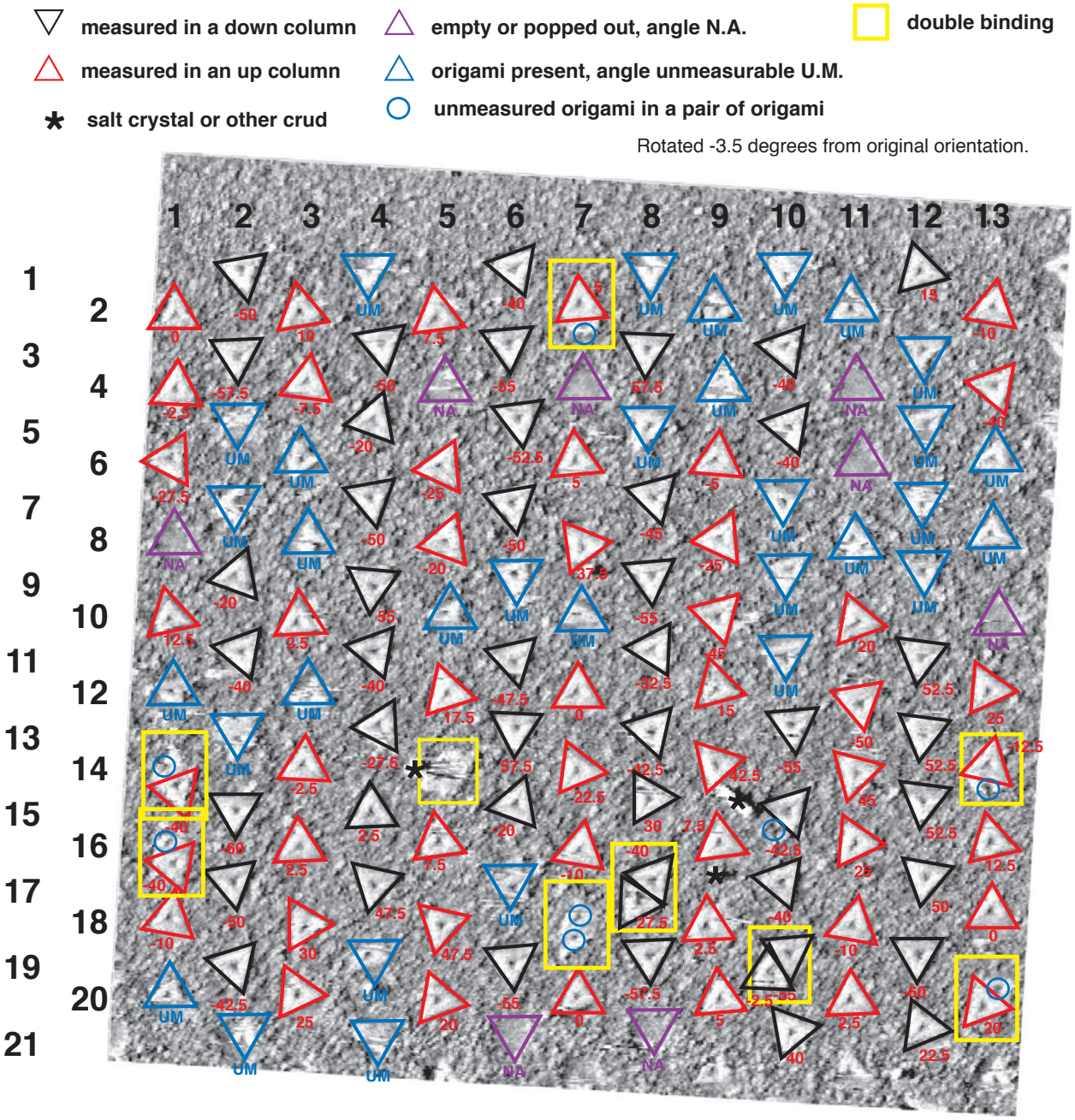

A	B	C	D	E
136 total sites	8 empty	9 doubles (6.6%)	32 unmeasured singles (poorly imaged, 23.5%)	87 total measured singles (63.7%)
70 up	6 up	7 up	13 up	44 up
66 down	2 down	2 down	19 down	43 down

A = B + C + D + E

9 additional triangles in doubles measured
5 up
4 down

94% of sites have at least one origami bound
88% of sites have apparently single origami bound
up angle: 3.64 +- 22.2 degrees down angle: -52.2 +- 20.4 degrees difference: -55.8 degrees

Figure S2: **DNA triangles on triangles patterned on a TMS/SiO_2 surface; etch condition 1. 125 mM $MgCl_2$/10×TAE** Annotations refer to orientation, number of origami at a site, etc.

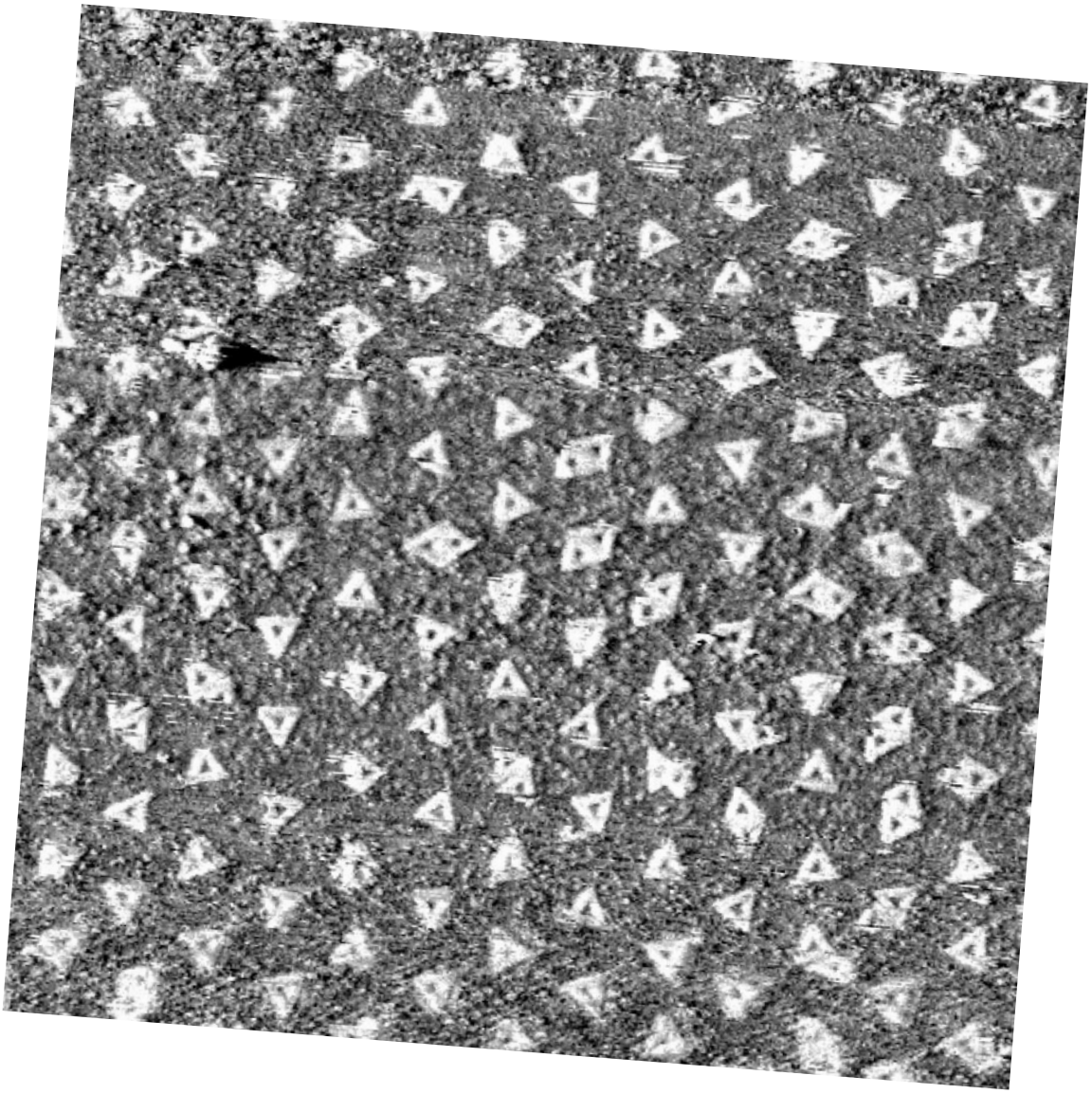

Figure S3: **DNA triangles on triangles patterned on a TMS/SiO_2 surface; etch condition 2. 125 mM $MgCl_2$/10×TAE** Unannotated 3 micron phase image. Phase runs from -2.5° (white) to 2.5° (black).

DOI: 10.1038/NNANO.2009.220

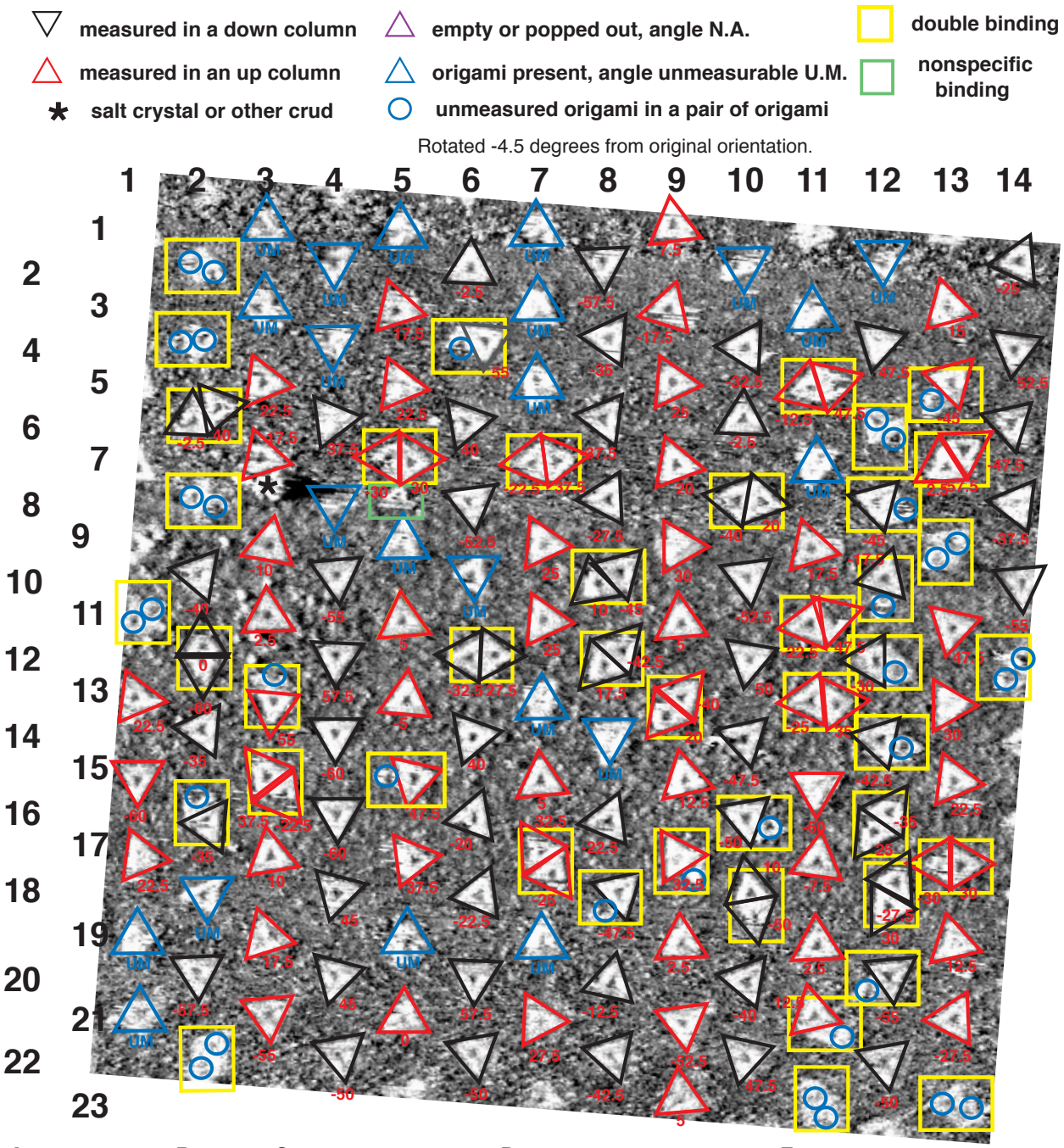

A	B	C	D	E
145 total sites	0 empty	43 doubles (29.7%)	23 unmeasured singles (poorly imaged, 15.9%)	80 total measured singles (55.2%)
73 up	0 up	19 up	14 up	40 up
72 down	0 down	24 down	8 down	40 down

A = B + C + D + E

51 additional triangles in doubles measured
25 up
26 down

1 nonspecifically bound triangle
100% of sites have at least one origami bound
71% of sites have apparently single origami bound
up angle: 18.0 +- 21.1 down angle: -49.4 +- 21.6 difference 67.4

Figure S4: **DNA triangles on triangles patterned on a TMS/SiO_2 surface; etch condition 2. 125 mM $MgCl_2$/10×TAE** Annotations refer to orientation, number of origami at a site, etc.

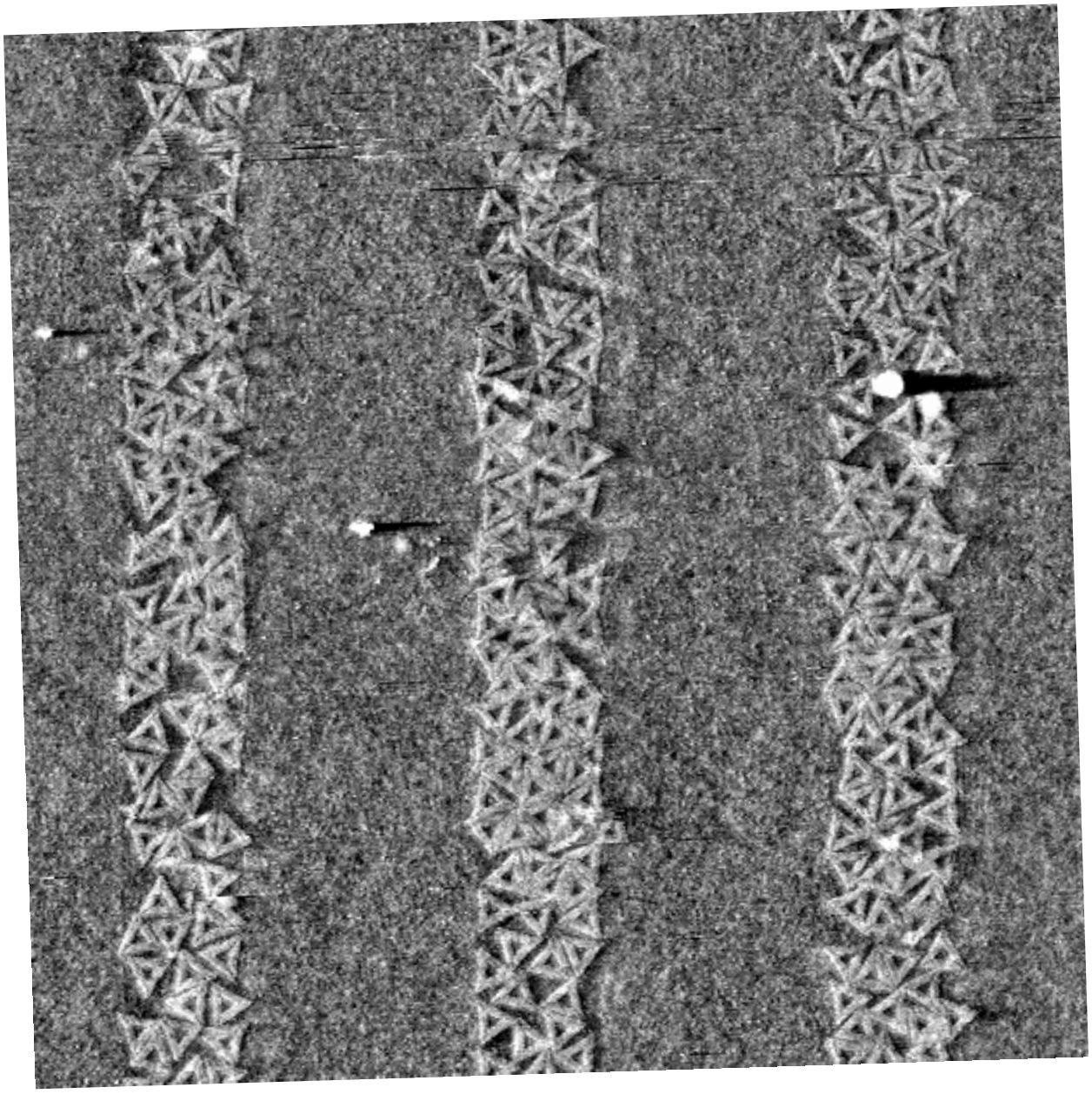

Figure S5: **DNA triangles on 350 nm optically patterned lines on a TMS/SiO_2 surface. 125 mM $MgCl_2$/10×TAE** Unannotated 3 micron phase image. Phase runs from -2.5° (white) to 2.5° (black).

DOI: 10.1038/NNANO.2009.220

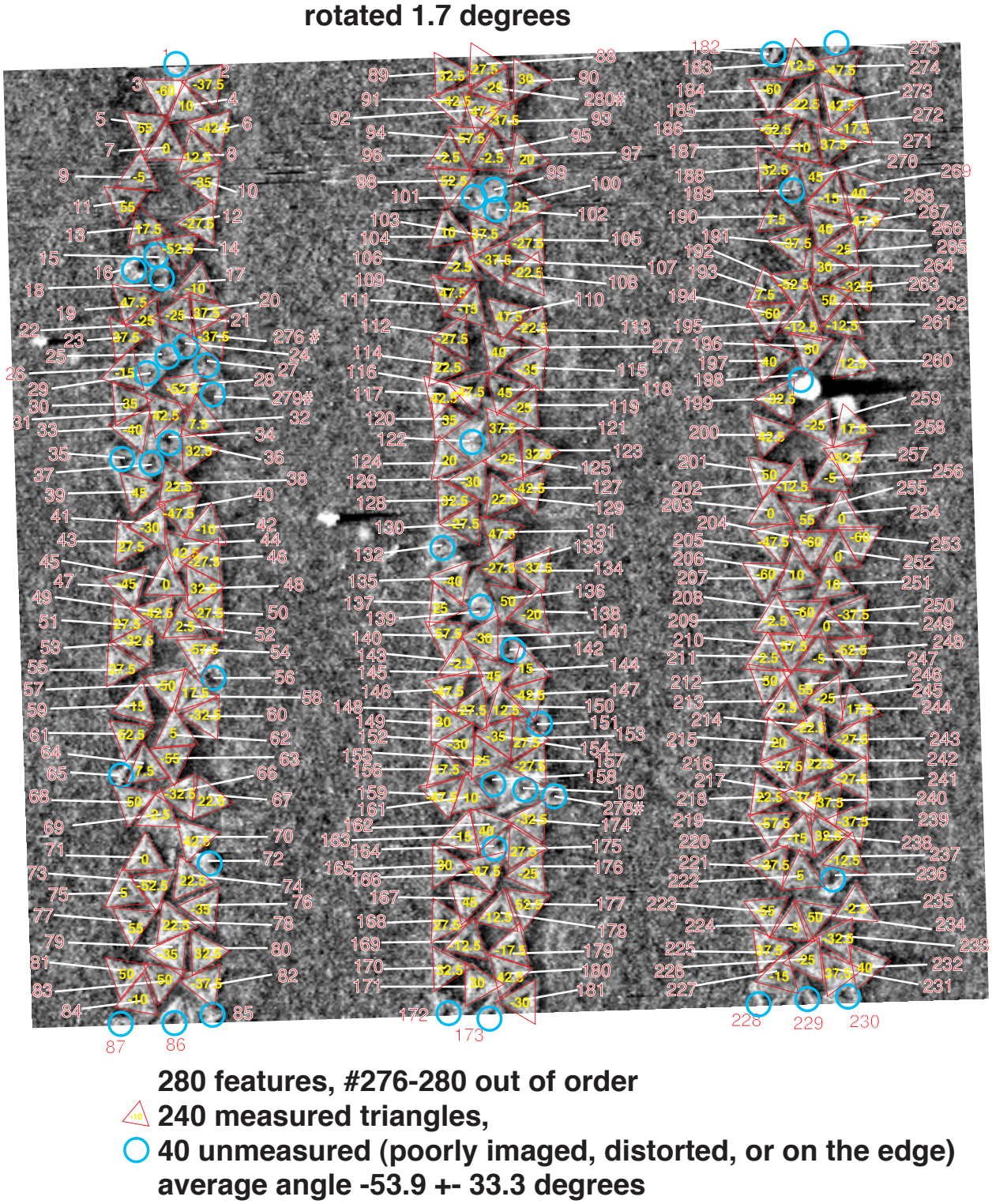

Figure S6: **DNA triangles on 350 nm optically patterned lines on a TMS/SiO_2 surface. 125 mM $MgCl_2$/10×TAE** Annotations refer to orientation, and whether a particular triangle was measured.

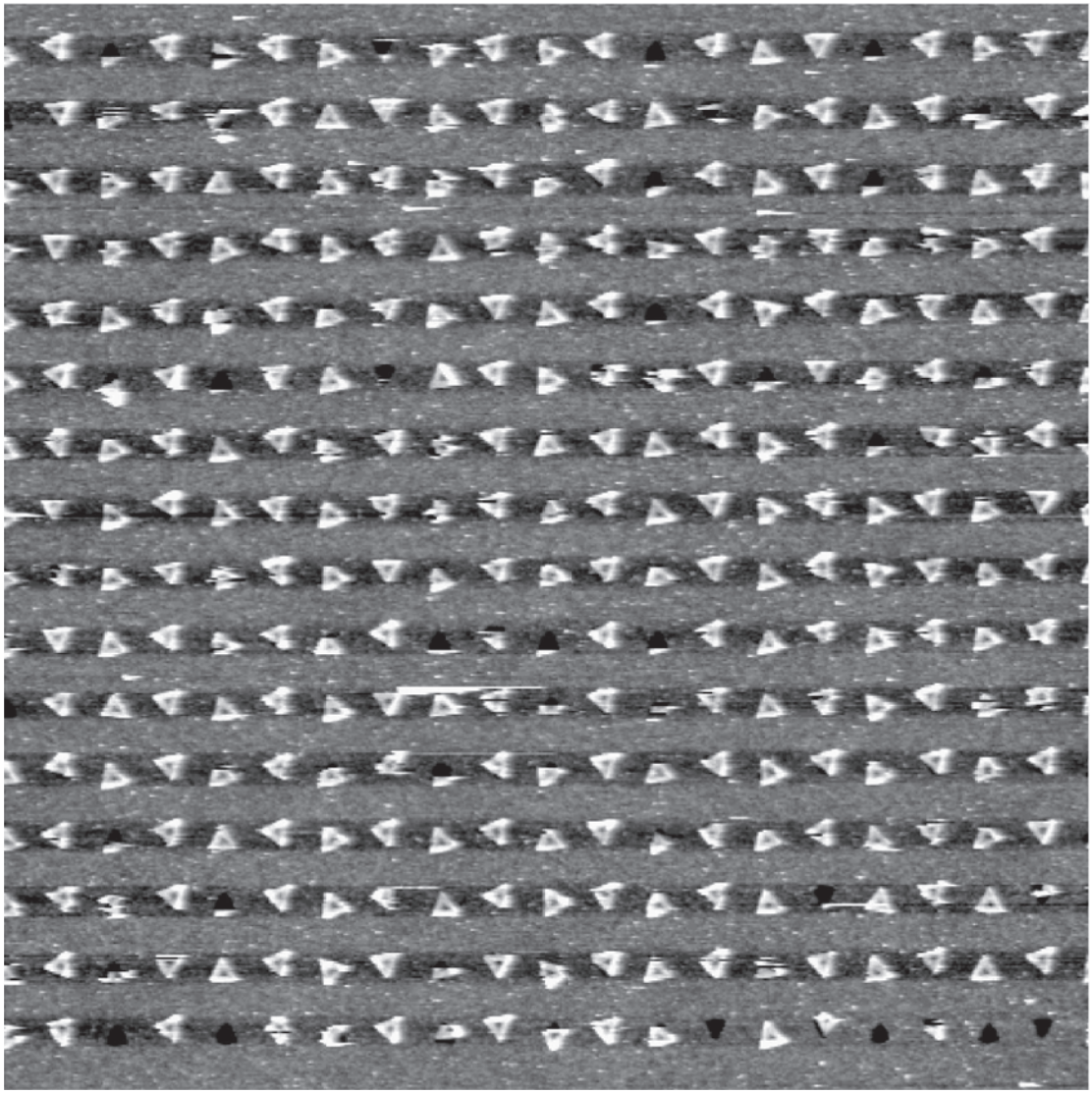

Figure S7: **DNA triangles on ∼1 nm deep triangles patterned on a DLC surface, 1st use. ∼114 mM $MgCl_2$ / 9.1×TAE.** Unannotated 5 μm height image. Height scale is 3 nm, and runs from black (0 nm) to white (3 nm).

DOI: 10.1038/NNANO.2009.220

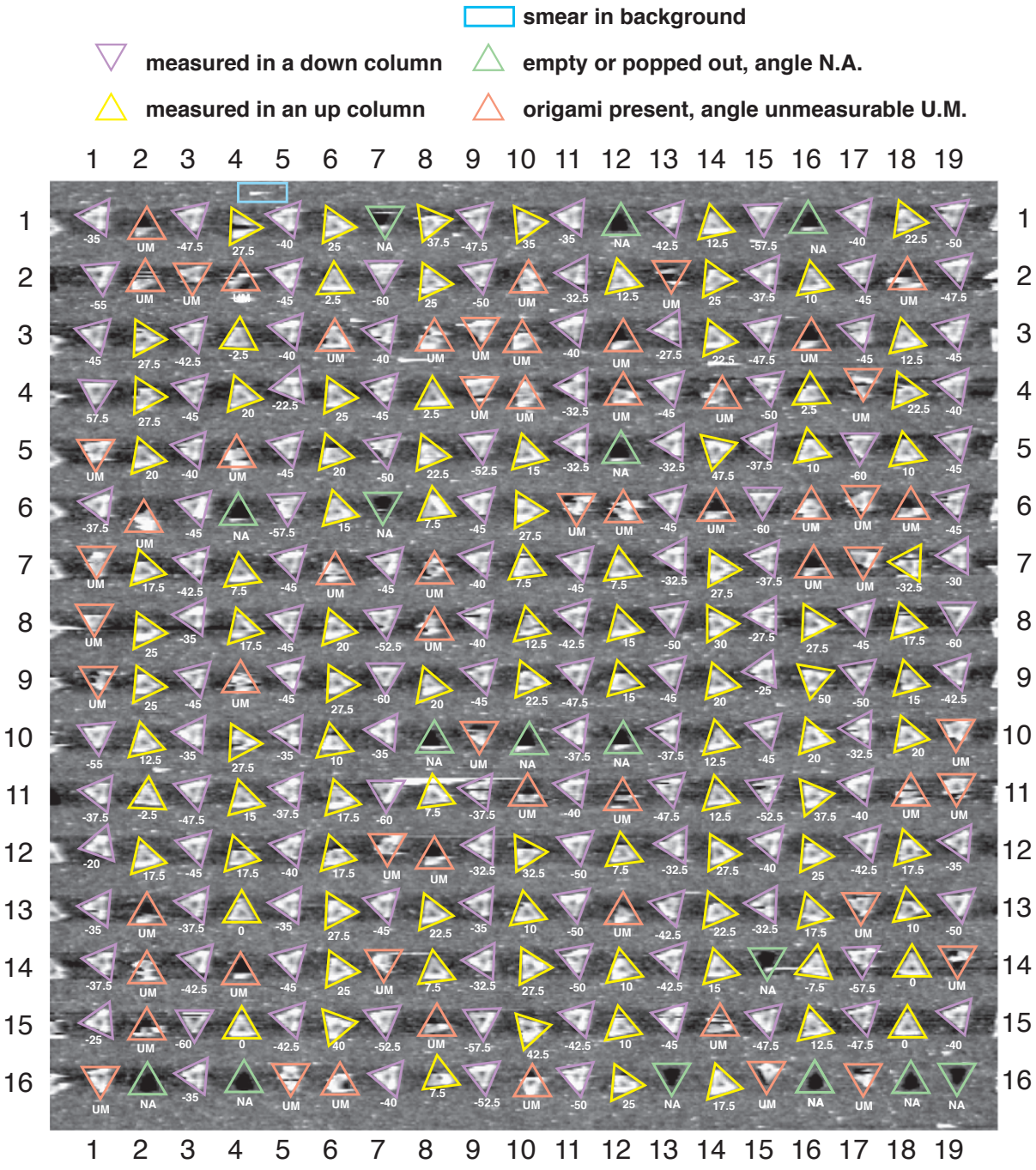

A	B	C	D	E
304 total sites	16 empty	0 doubles	60 unmeasured singles (poorly imaged, 19.7%)	228 total measured singles (75%)
144 up	11 up	0 up	37 up	96 up
160 down	5 down	0 down	23 down	132 down

95% of sites have an origami present
75% of sites have an origami whose orientation is measurable
(observable central hole and 2 sides at ~60 degrees, or 3 sides mutually ~60 apart)

up angle: 17.5 +- 12.0 degrees down angle: -43.1 +- 8.4 degrees difference: 60.6 degrees

Figure S8: **DNA triangles on ~1 nm deep triangles patterned on a DLC surface, 1st use. ~114 mM $MgCl_2$ / 9.1×TAE.** Annotations refer to orientation, number of origami at a site, etc.

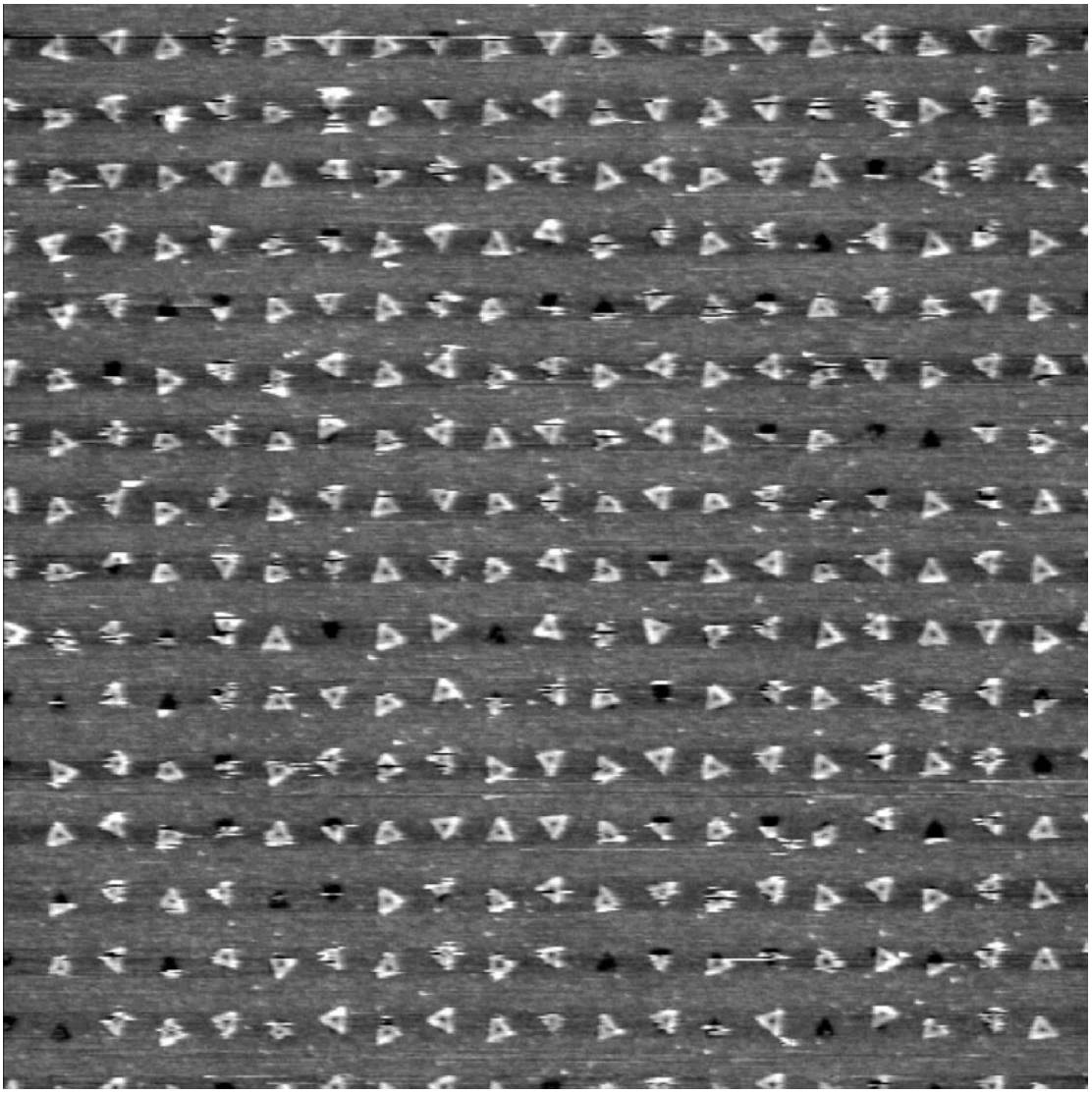

Figure S9: **DNA triangles on ∼1 nm deep triangles patterned on a DLC surface, 2nd use. ∼114 mM $MgCl_2$ / 9.1×TAE.** Unannotated 5 μm height image. Height scale is 3 nm, and runs from black (0 nm) to white (3 nm).

DOI: 10.1038/NNANO.2009.220

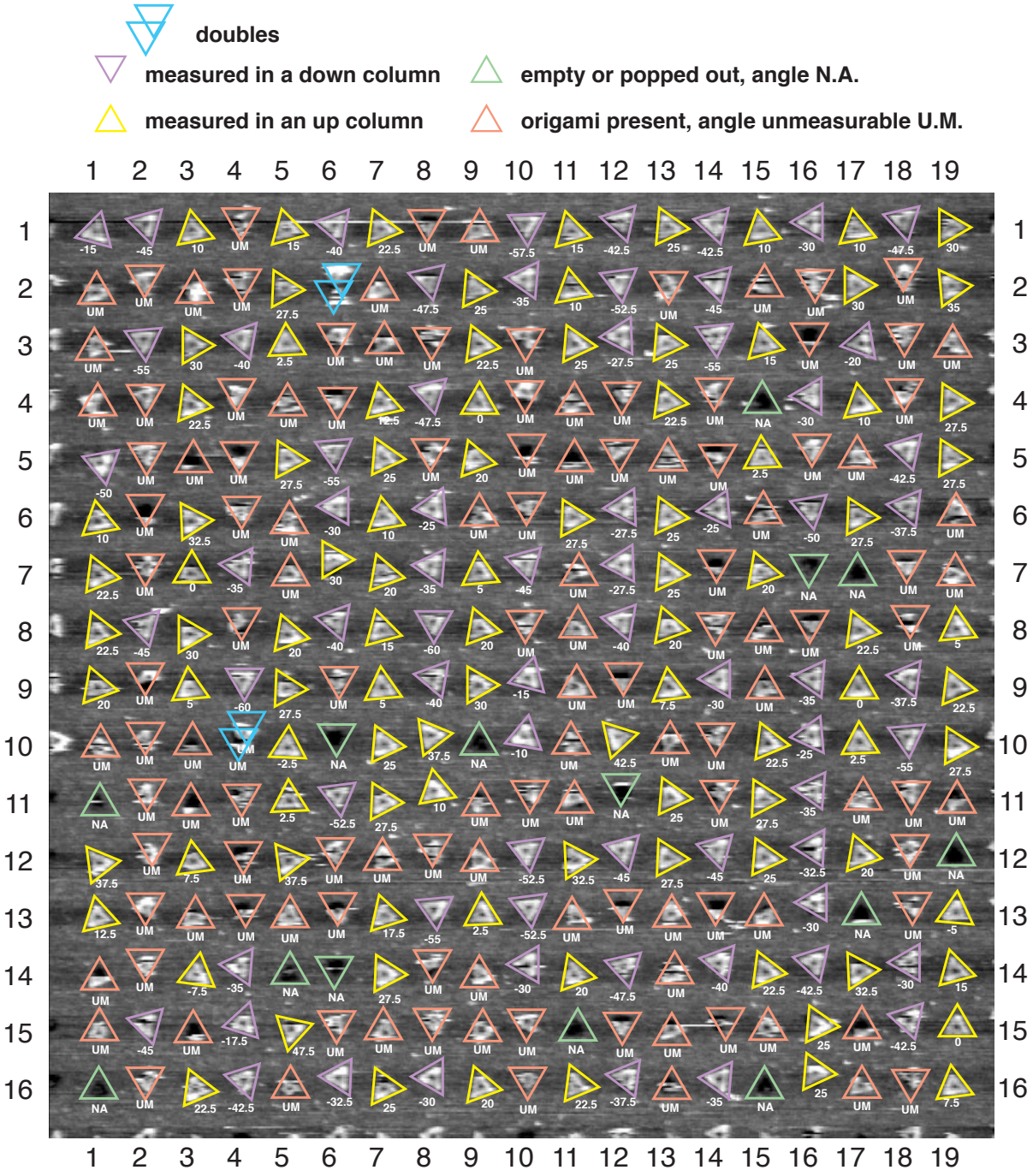

A	B	C	D	E
304 total sites	14 empty (4.6%)	2 doubles (.66%)	123 unmeasured singles (poorly imaged, 40.5%)	165 total measured singles (54.3%)
160 up	10 up	0 up	56 up	94 up
144 down	4 down	2 down	67 down	71 down

95.4% of sites have one or more origami present; 94.7% single origami (but many are partial)
54.3% of sites have a single origami whose orientation was measured
(observable central hole and 2 sides at ~60 degrees, or 3 sides mutually ~60 apart)

up angle: 18.5 +- 13.1 degrees down angle: -42.3 +- 17.5 degrees difference: 60.9 degrees

Figure S10: **DNA triangles on ~1 nm deep triangles patterned on a DLC surface, 2nd use. ~114 mM $MgCl_2$ / 9.1×TAE.** Annotations refer to orientation, number of origami at a site, etc.

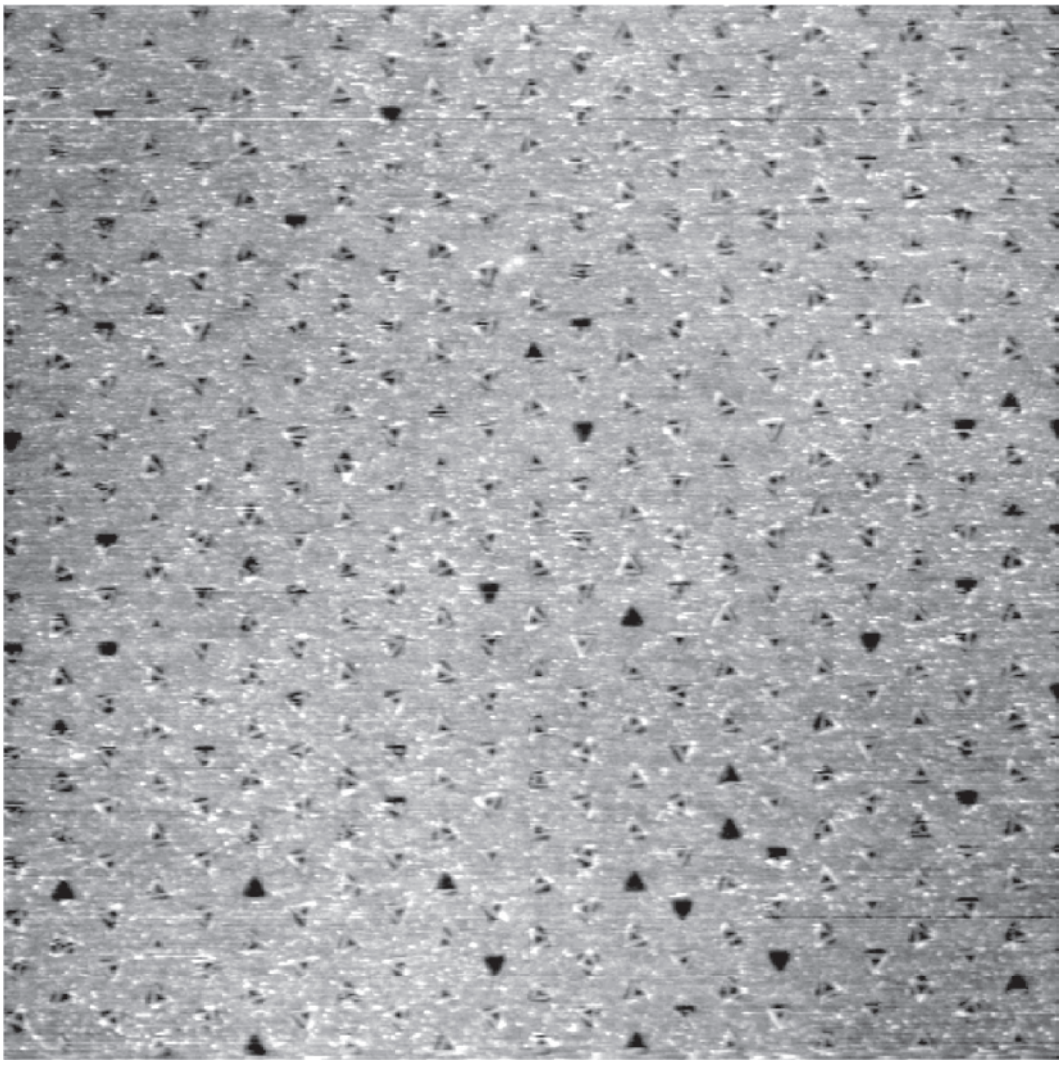

Figure S11: **DNA triangles on ∼1.5 nm deep triangles patterned on a DLC surface. ∼114 mM $MgCl_2$ / 9.1×TAE.** Unannotated 5 micron height image. Height scale is 3 nm, and runs from black (0 nm) to white (3 nm). Triangles fit more deeply into features, almost flush with the background surface and so exhibit less contrast than images for which the feature depth is ∼1 nm, such as Fig. S7.

DOI: 10.1038/NNANO.2009.220

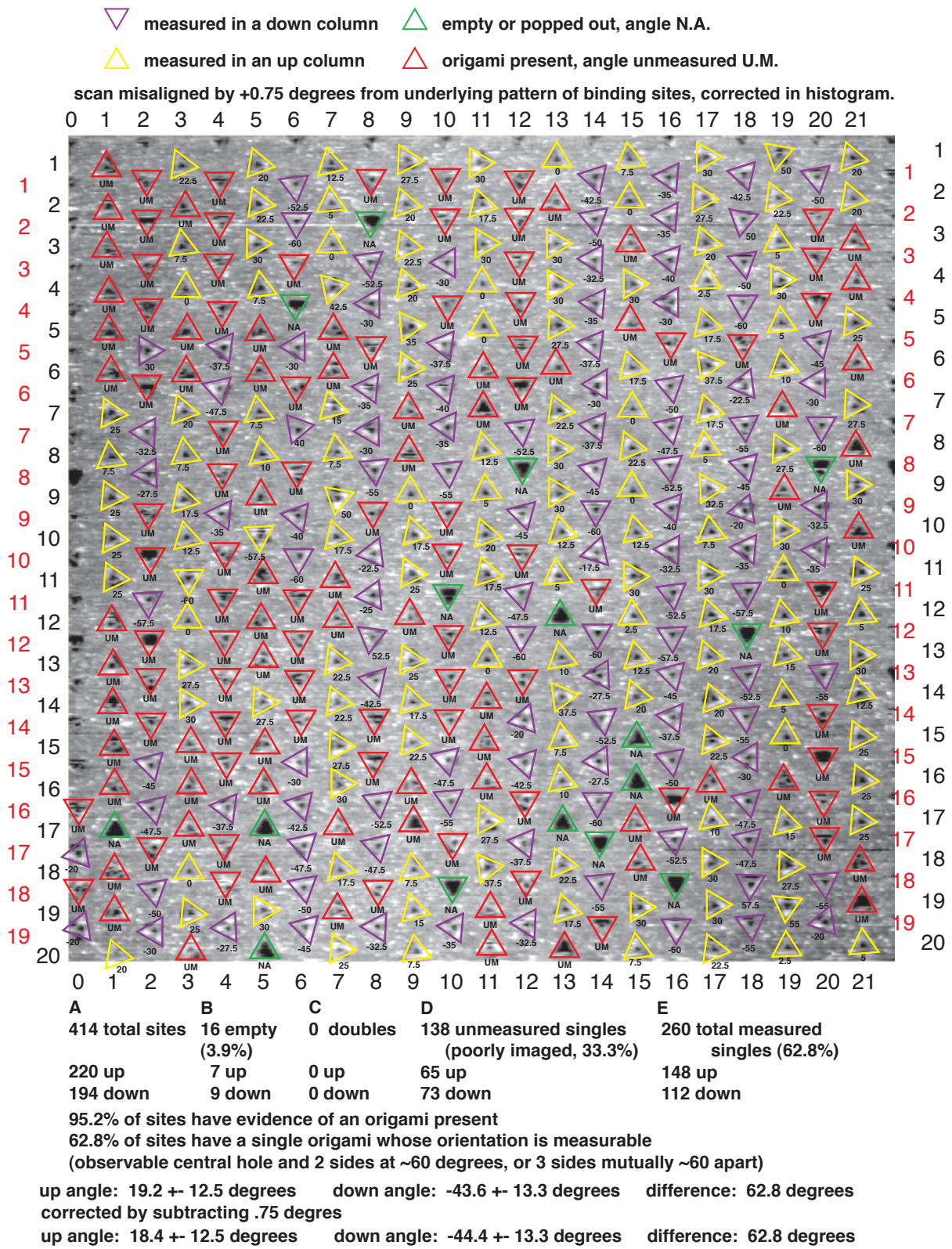

Figure S12: **DNA triangles on ~1.5 nm deep triangles patterned on a DLC surface. ~114 mM $MgCl_2$ / 9.1×TAE.** Annotations refer to orientation, number of origami at a site, etc. The additional 0.5 nm depth of the features does not significantly affect the quality of alignment. As in other experiments, a 16–18 degree offset is observed. Triangular features vary in size but some are up to ~ 120 nm, slightly larger than in Figs. S7–S10 (~ 110 nm); this also does not significantly affect the quality of alignment.

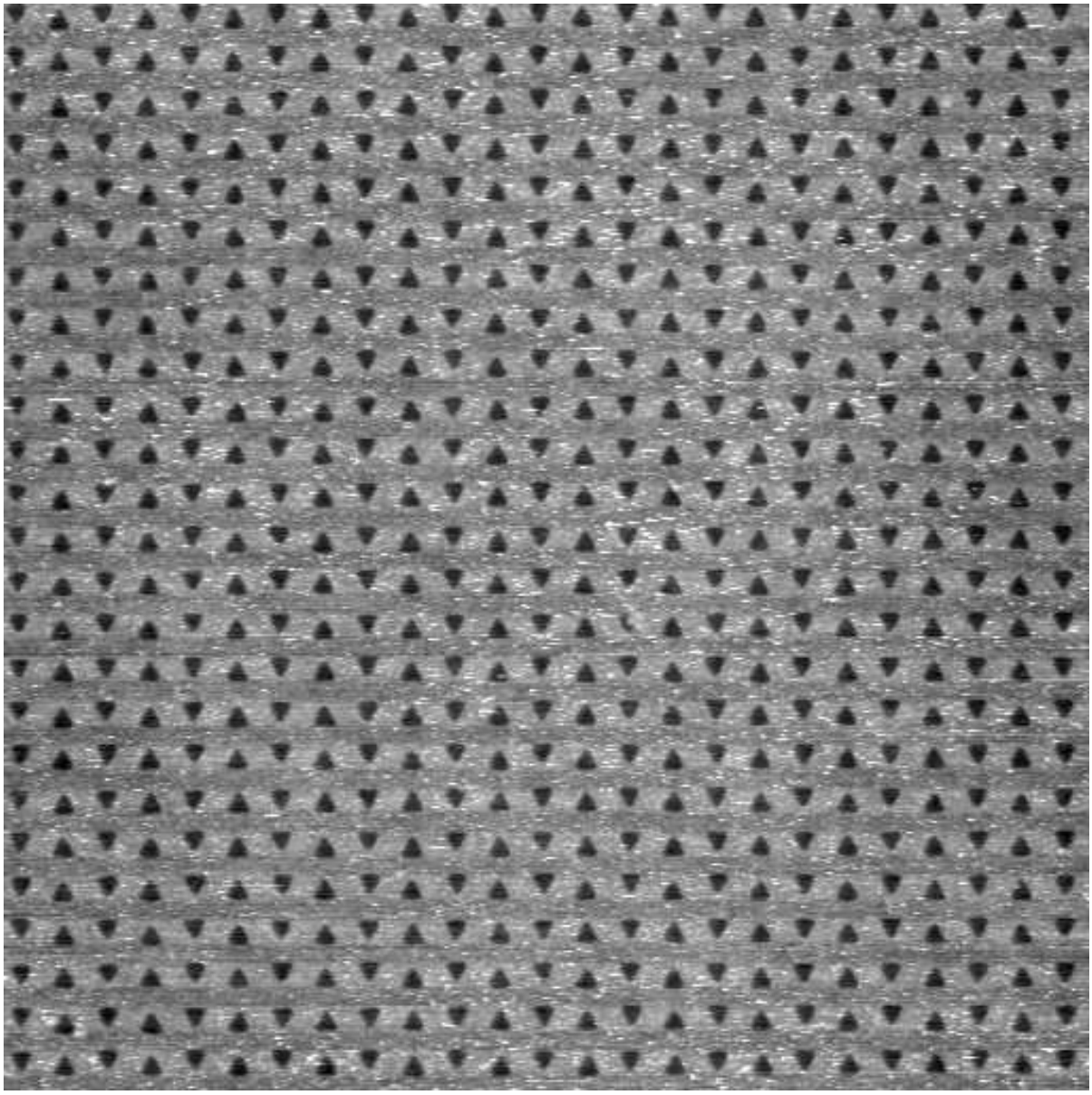

Figure S 13: **DLC surface treated with DNA triangles in their formation buffer, ∼69 mM $MgCl_2$ / 5.5×TAE.** DNA origami do not stick under these conditions. Unannotated 5 micron height image. Height scale is 3 nm, and runs from black (0 nm) to white (3 nm).

DOI: 10.1038/NNANO.2009.220

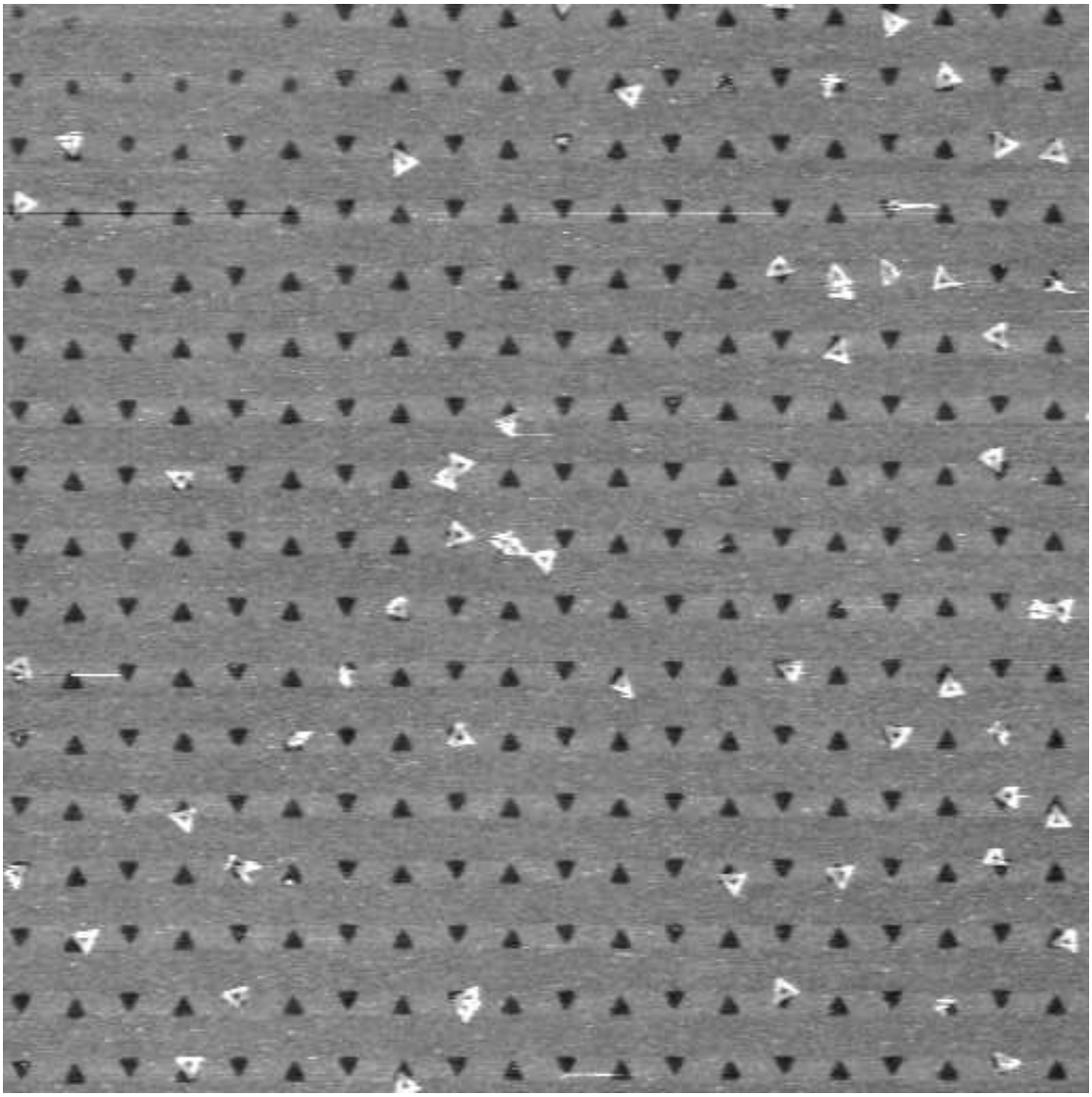

Figure S14: **DNA triangles on triangles patterned on a DLC surface in 1 M Mg^{2+} / 10× TAE.** Unannotated 5 micron height image. Height scale is 3 nm, and runs from black (0 nm) to white (3 nm).

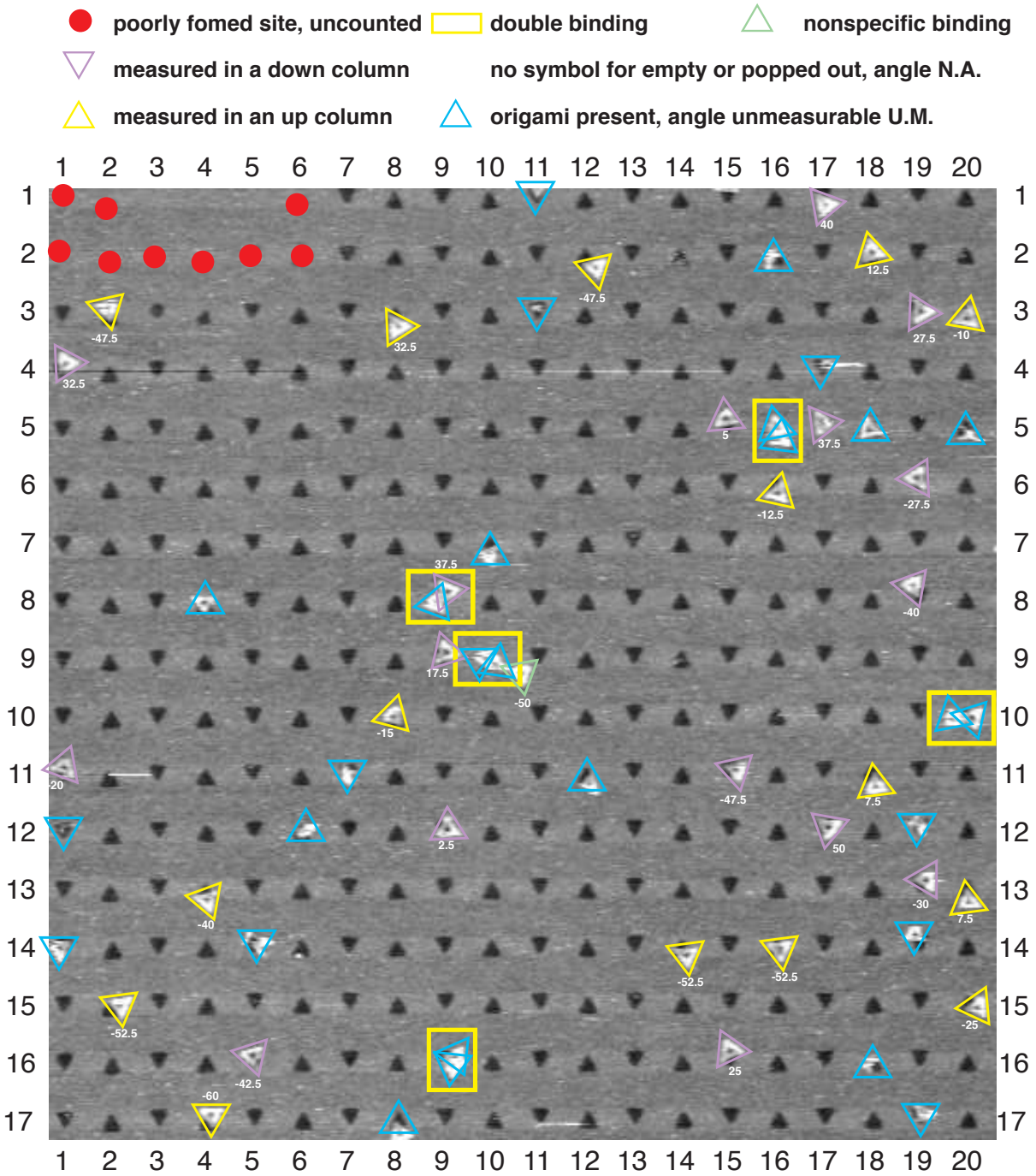

A	B	C	D	E
328 total sites	176 empty	5 doubles (1.5%)	19 unmeasured singles (poorly imaged, 5.8%)	30 total measured singles (9.2%)
164 up	137 up	3 up	9 up	15 up
164 down	137 down	2 down	10 down	15 down

1 nonspecifically bound triangle
16.1% of sites have at least one origami present
9.2% of sites have a single origami whose orientation is measurable
(observable central hole and 2 sides at ~60 degrees, or 3 sides mutually ~60 apart)
up angle: -31.7 +- 29.2 degrees down angle: 47.7 +- 32 degrees difference: 79.3 degrees

Figure S15: **DNA triangles on triangles patterned on a DLC surface in 1 M Mg^{2+} / 10× TAE.** Annotations refer to orientation, number of origami at a site, etc. Fit to binding sites is not maximized: single origami do not center on binding sites and doubles are not aligned edge to edge as on TMS/SiO_2 (Fig. S4).

DOI: 10.1038/NNANO.2009.220

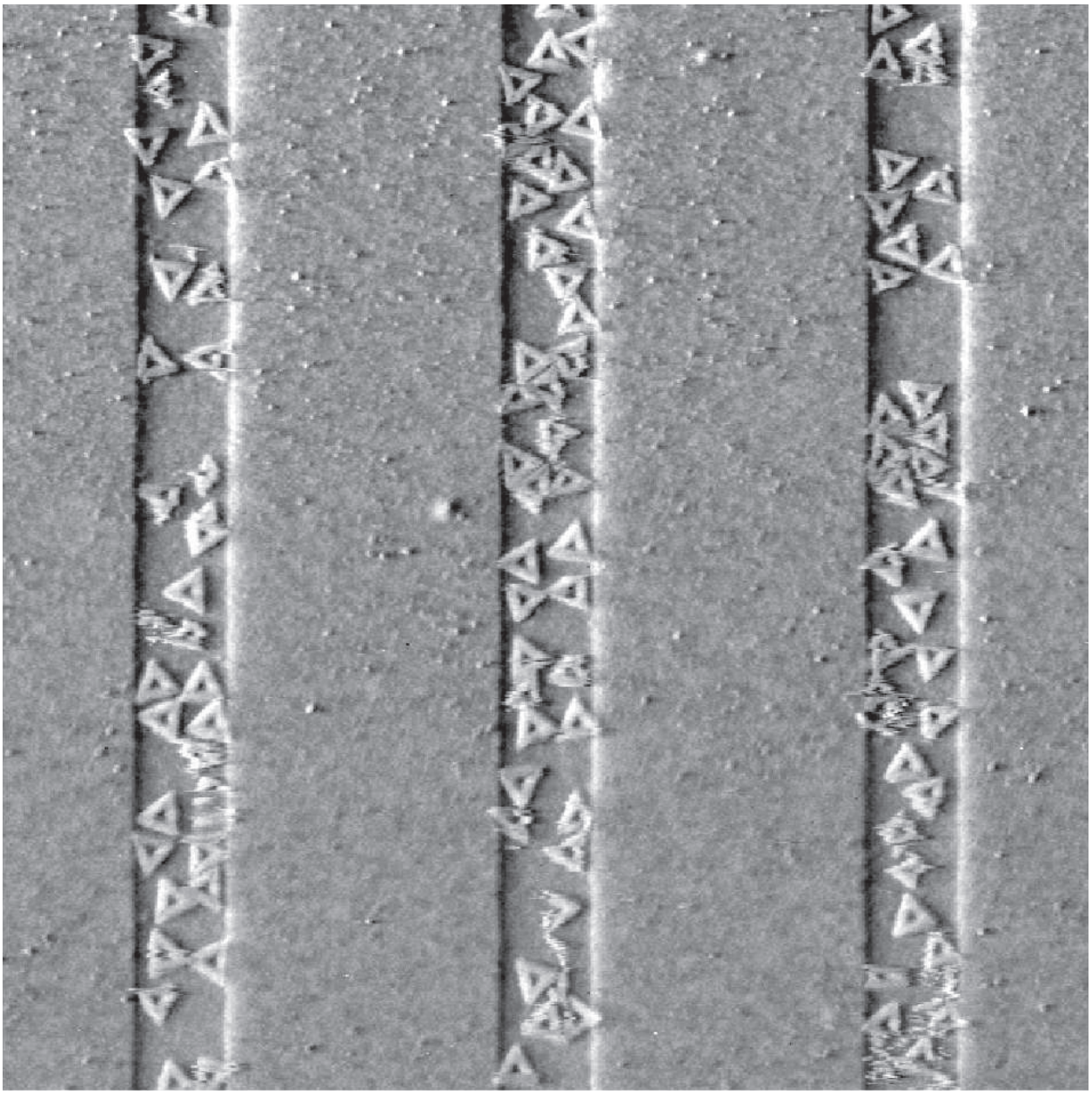

Figure S16: **DNA triangles on 200 nm lines patterned on a DLC surface.** Unannotated 5 micron phase image. Phase runs from -2.5° (white) to 2.5° (black).

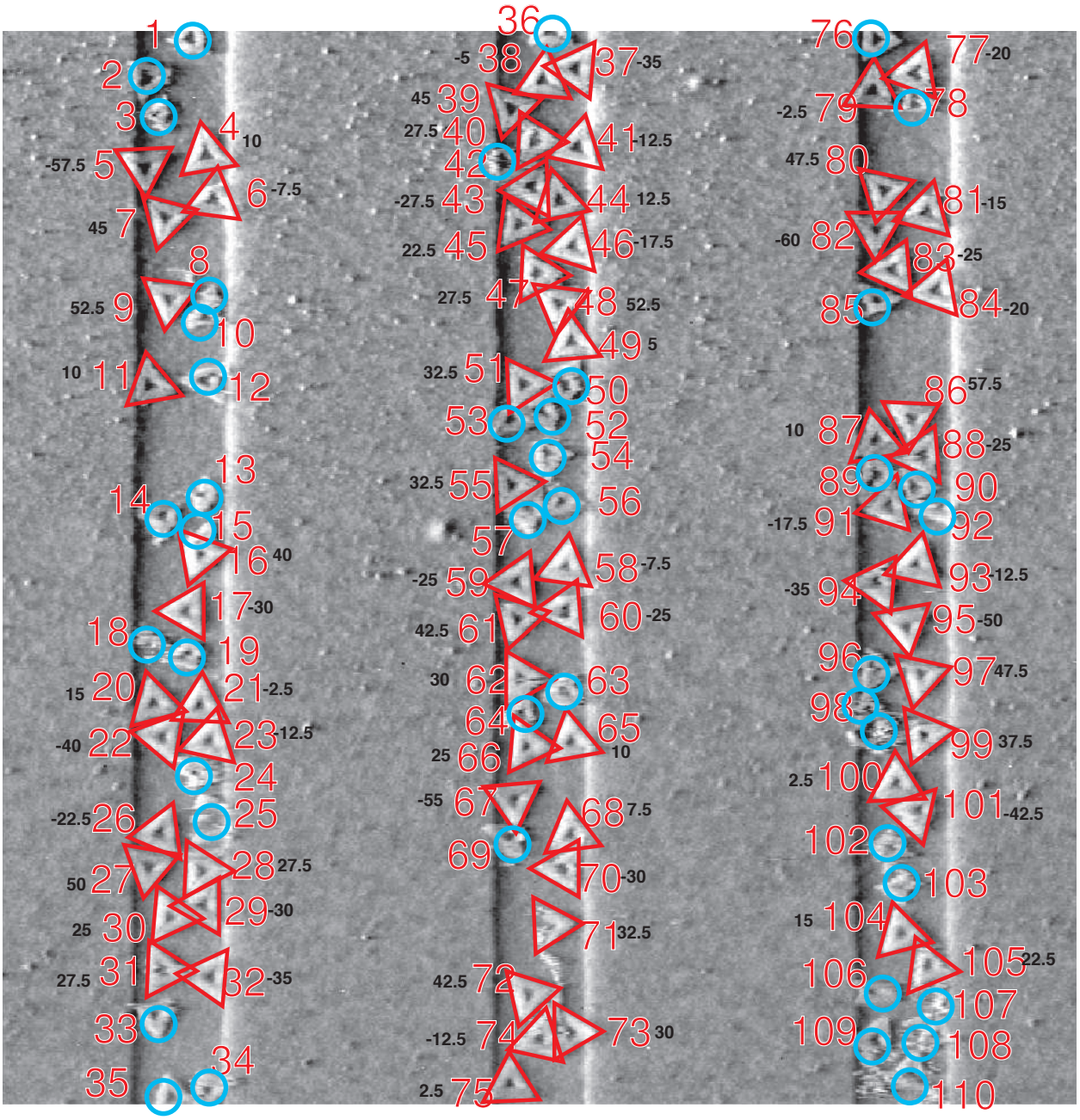

Figure S17: **DNA triangles on 200 nm lines patterned on a DLC surface.** Annotations refer to orientation, number of origami at a site, etc.

DOI: 10.1038/NNANO.2009.220

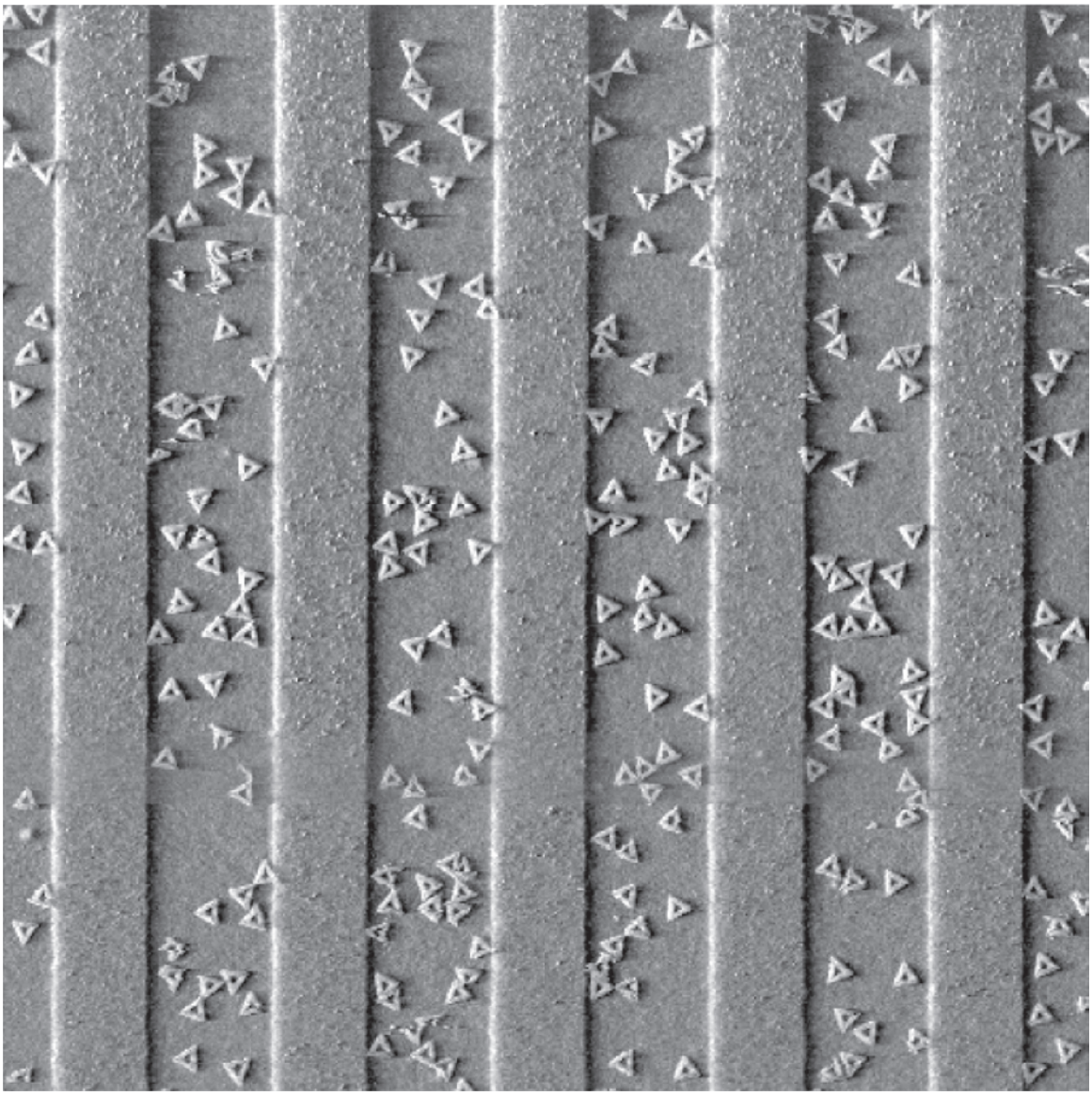

Figure S18: **DNA triangles on 500 nm lines patterned on a DLC surface.** Unannotated 5 micron phase image. Phase runs from -2.5° (white) to 2.5° (black).

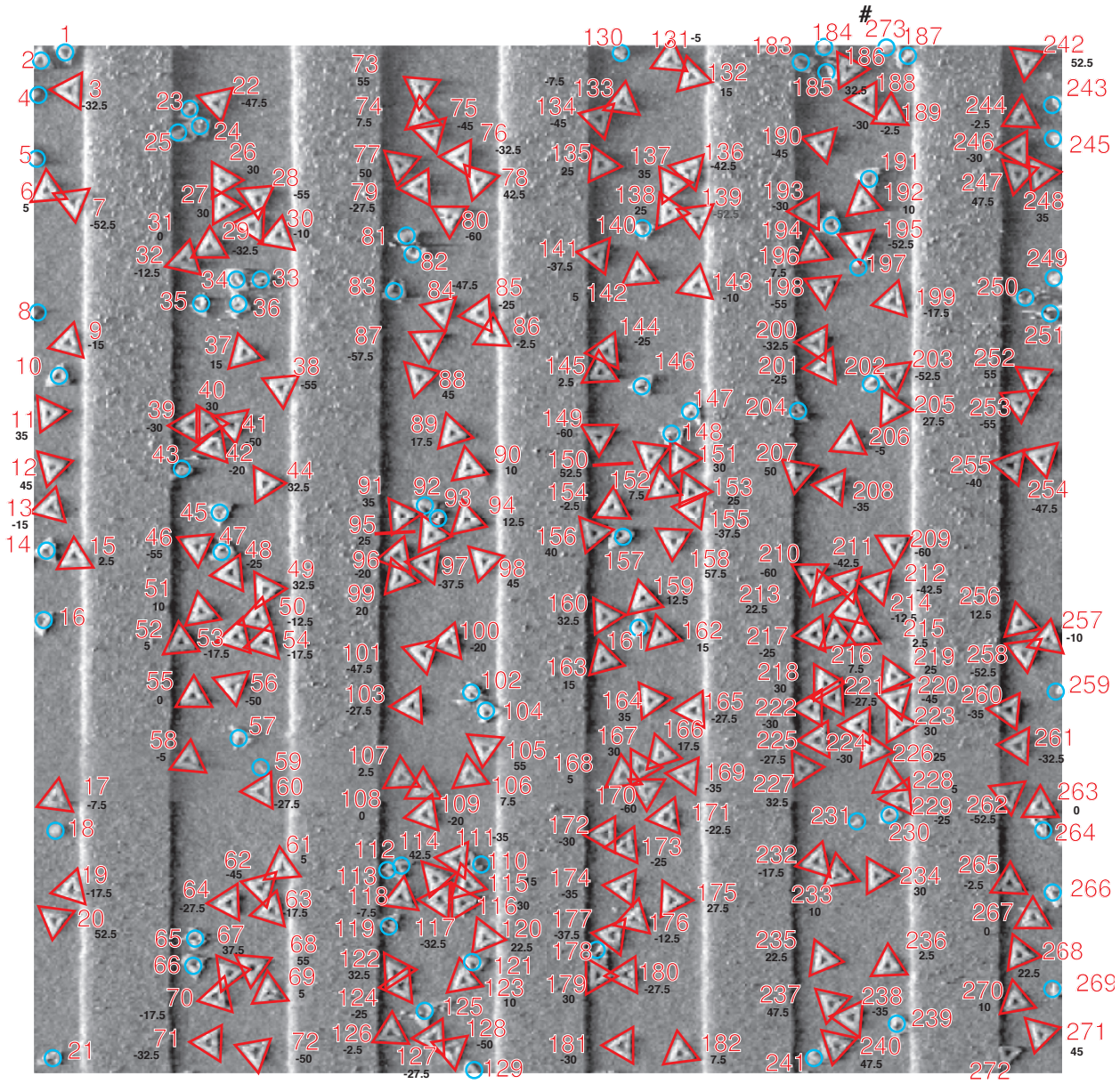

Figure S19: **DNA triangles on 500 nm lines patterned on a DLC surface.** Annotations refer to orientation, number of origami at a site, etc.

DOI: 10.1038/NNANO.2009.220

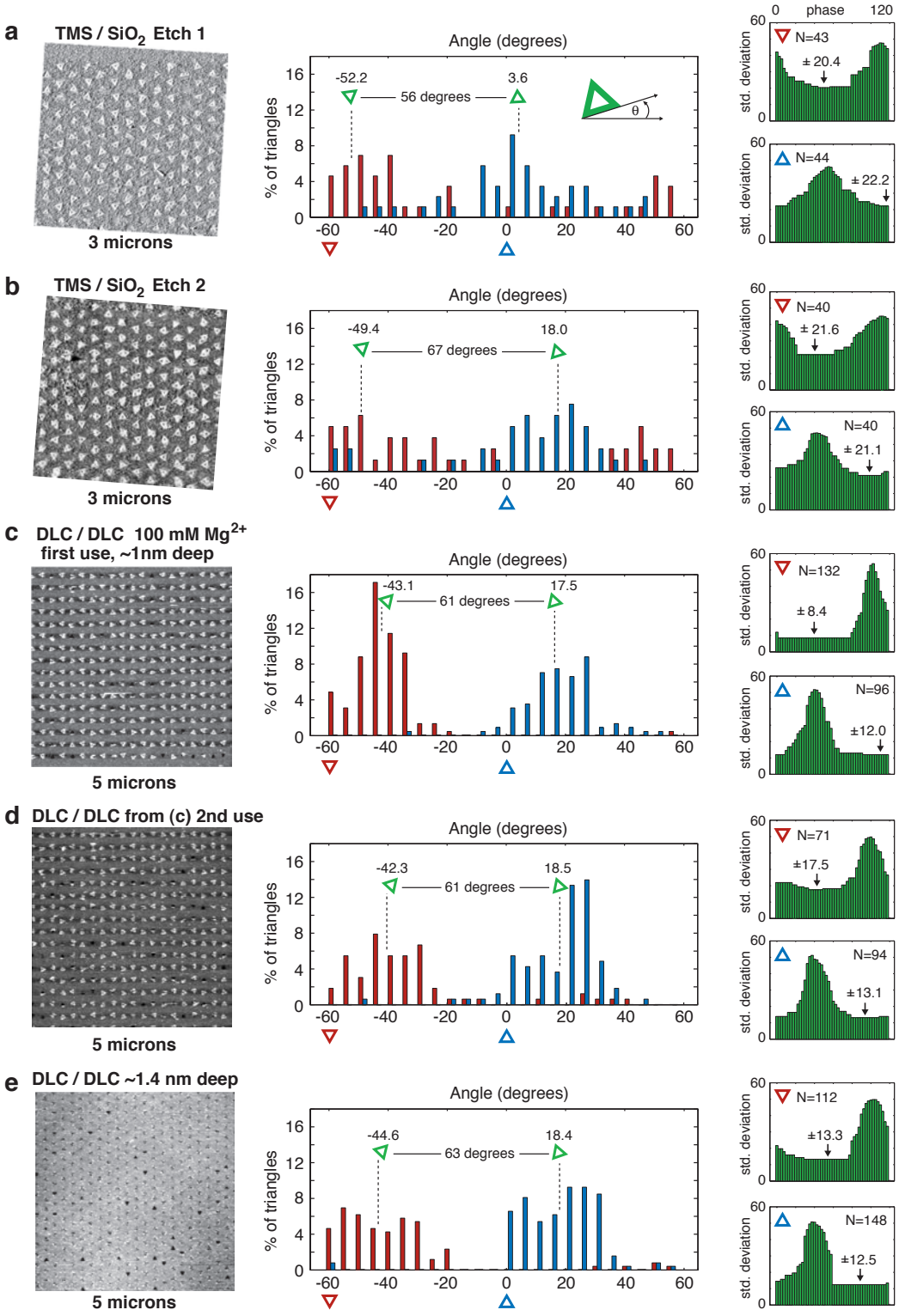

Figure S 20: **Histograms showing the number of DNA triangles of a given angle with respect to sticky triangular features.** Positions of green triangles marking peaks are approximate. Triangles on TMS/SiO_2 in (**a**) and (**b**) show a moderate degree of orientation, with 1 standard deviation (s.d.) from peaks of ~20°. See supp. Section 4 for differences between etch conditions 1 and 2. Triangles on DLC/DLC with features ~1 nm deep (**c**) show a much higher degree of orientation with 1 s.d. from peaks of ~10° (average of up and down distributions). After a piranha etch and reuse, the orientation on DLC/DLC (**d**) is mildly degraded (roughly 15°, average of up and down distributions). Triangles on DLC/DLC with features ~1.5 nm deep (**e**) show similar (~13°, average of up and down distributions). Green histograms show s.d. as a function of the phase of a cyclic permutation of the corresponding angle histogram. Arrows indicate minima in the s.d. which, for these data, form a single continuous plateau.

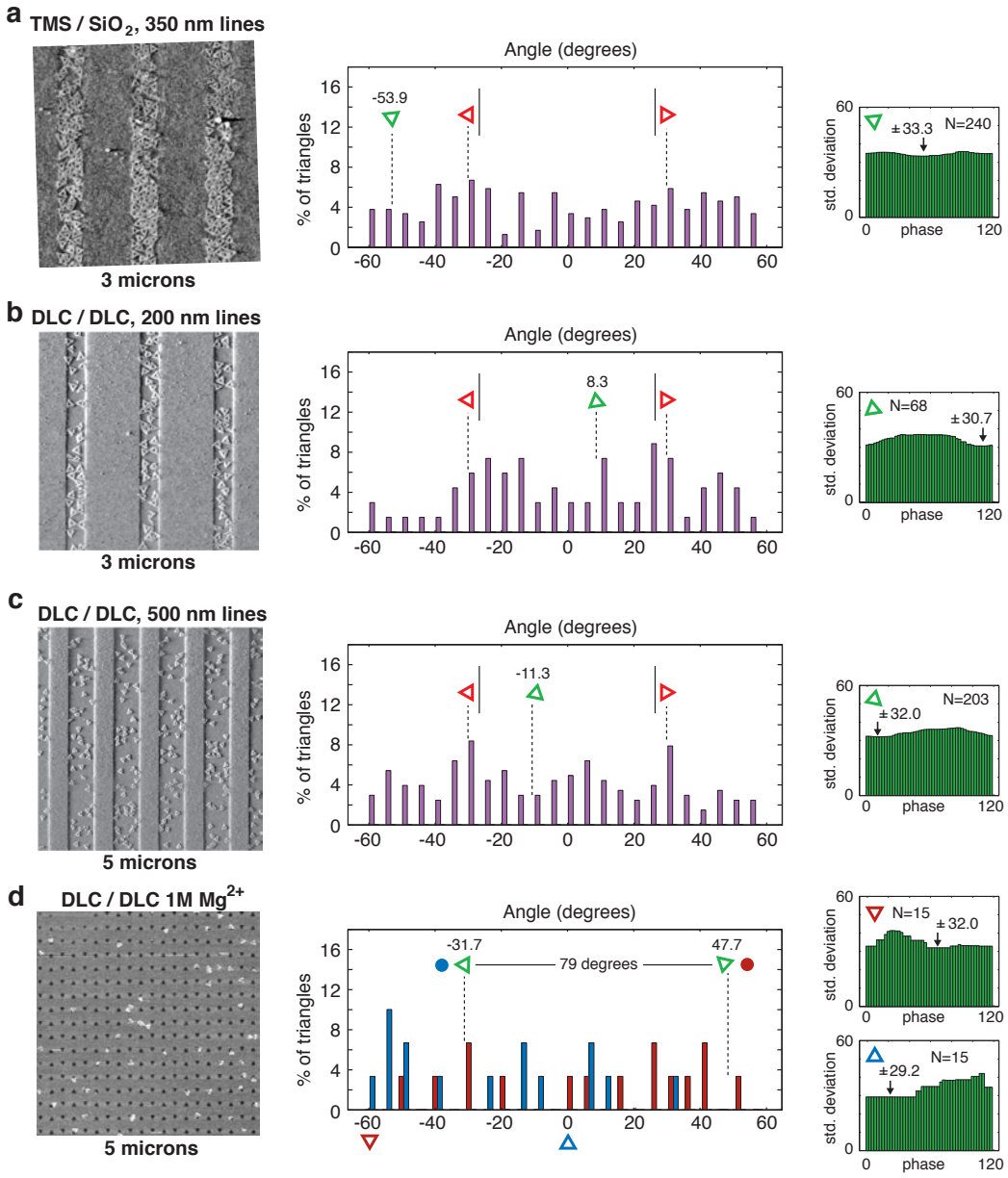

Figure S21: **Histograms showing the number of DNA triangles of a given angle, examples of random distributions.** No preferred orientation is observed for DNA triangles on TMS/SiO_2 patterned optically with 350 nm lines (**a**), or on DLC/DLC e-beam patterned with 200 nm (**b**) or 500 nm (**c**) wide lines. Red triangles mark orientations where peaks would have been expected to be observed, had the triangles aligned to the walls of the line features; no such peaks are obvious, even when triangles are almost close-packed, as in (**a**). (For **a**, it might appear by eye that close packing causes the triangles to align against the edges of line features but the data do not bear this out.) Single minima in the histograms of standard deviation (green histograms at right) as a function of the phase of the cyclic permutation of the angle histogram are coincidental for (**b**) and (**c**); random distributions on these sample sizes often have single minima but often have more than one minima as does (**a**). For (**a**) we use the minima of lowest standard deviation to characterize the distribution. (**d**), triangles on DLC/DLC with 1 M Mg^{2+} show no orientational selectivity. Note that the best fit peaks for triangle orientation give orientations that are 79° (or equivalently 41°) apart, not the 60° desired. Because peak assignments are not obvious as in previous histograms in Fig. S20, a blue dot indicates the best fit peak in the up-oriented columns, and a red dot the best fit peak in the down-oriented columns.

DOI: 10.1038/NNANO.2009.220

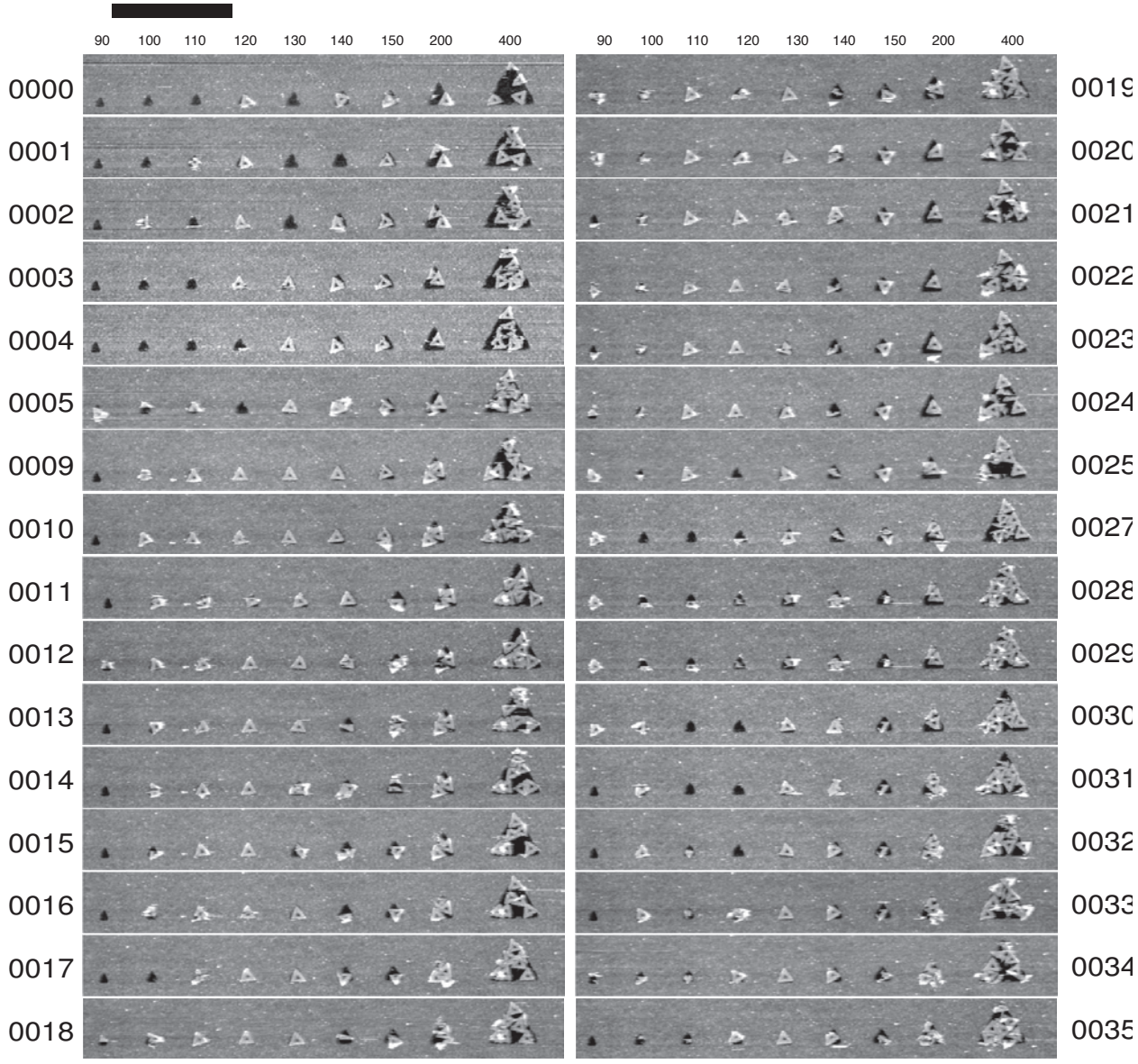

Figure S22: **AFM movie of DNA origami triangles binding to variously sized triangles on a DLC surface; first ~ 70 minutes.** Scale bar, 1 micron. The first (90 nm) site switches between empty and filled seven times over the course of the movie.

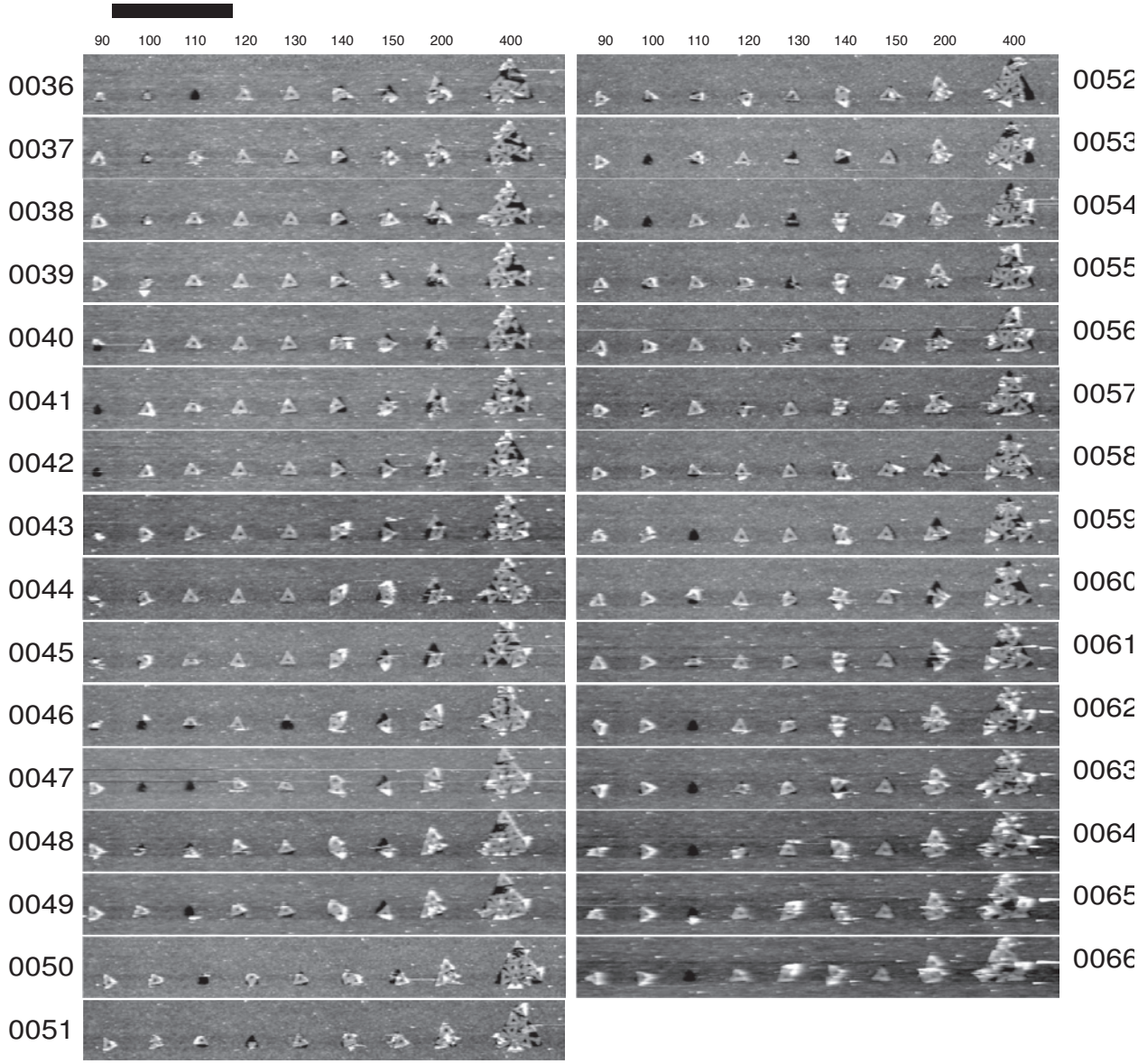

Figure S23: **AFM movie of DNA origami triangles binding to variously sized triangles on a DLC surface; minute ~ 70 to minute ~ 135.** Scale bar, 1 micron. Qualitatively the 120 and 130 nm sites maintain the best orientation.

DOI: 10.1038/NNANO.2009.220

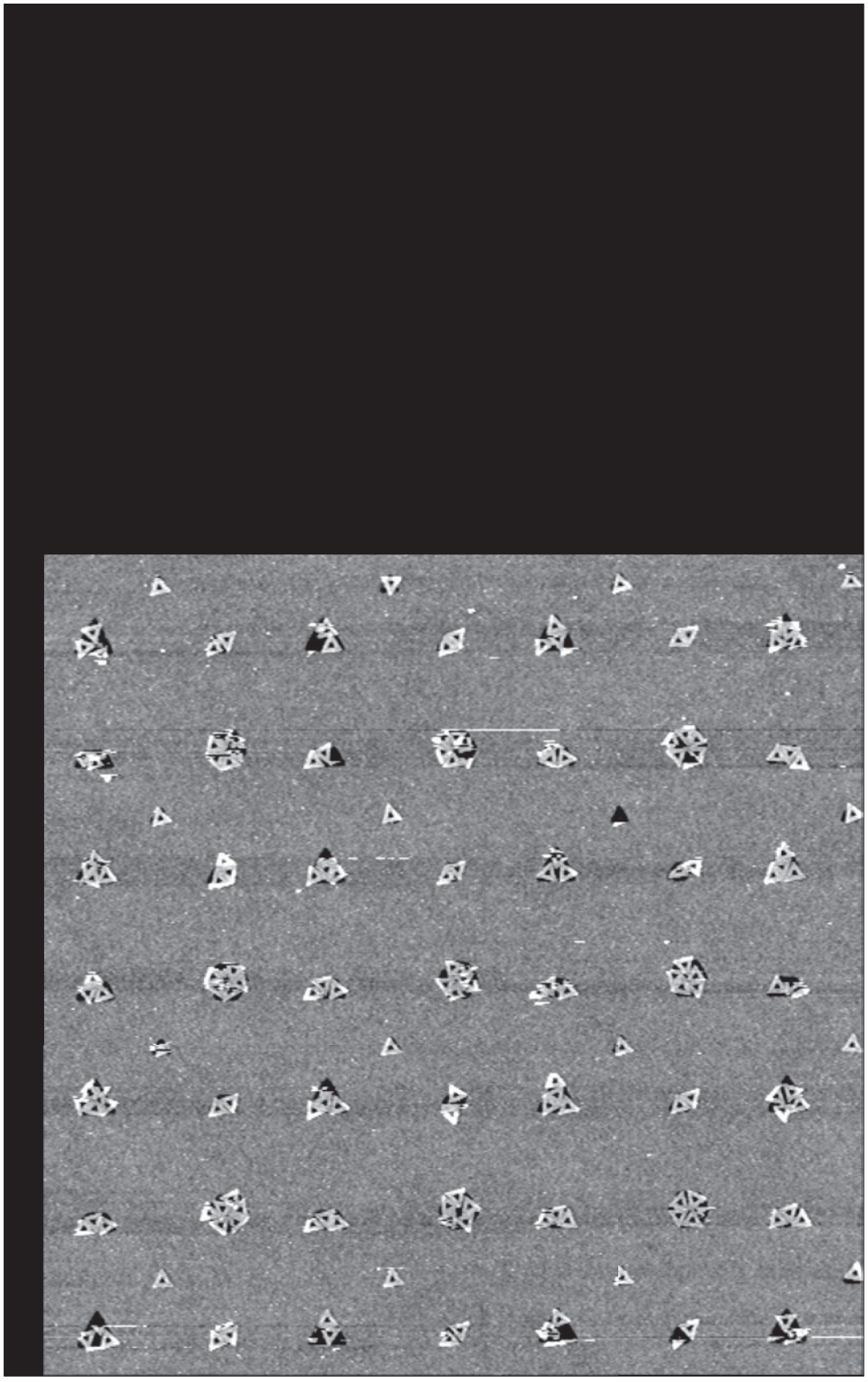

Figure S24: **Triangles on a DLC surface patterned with multiple shapes based on a ∼121 nm unit-sized binding site.** Unannotated 3 μm height image. Height scale is 3 nm, and runs from black (0 nm) to white (3 nm). Qualitatively, it appears that a small angular offset (+15°) is observed, even at multi-origami binding sites.

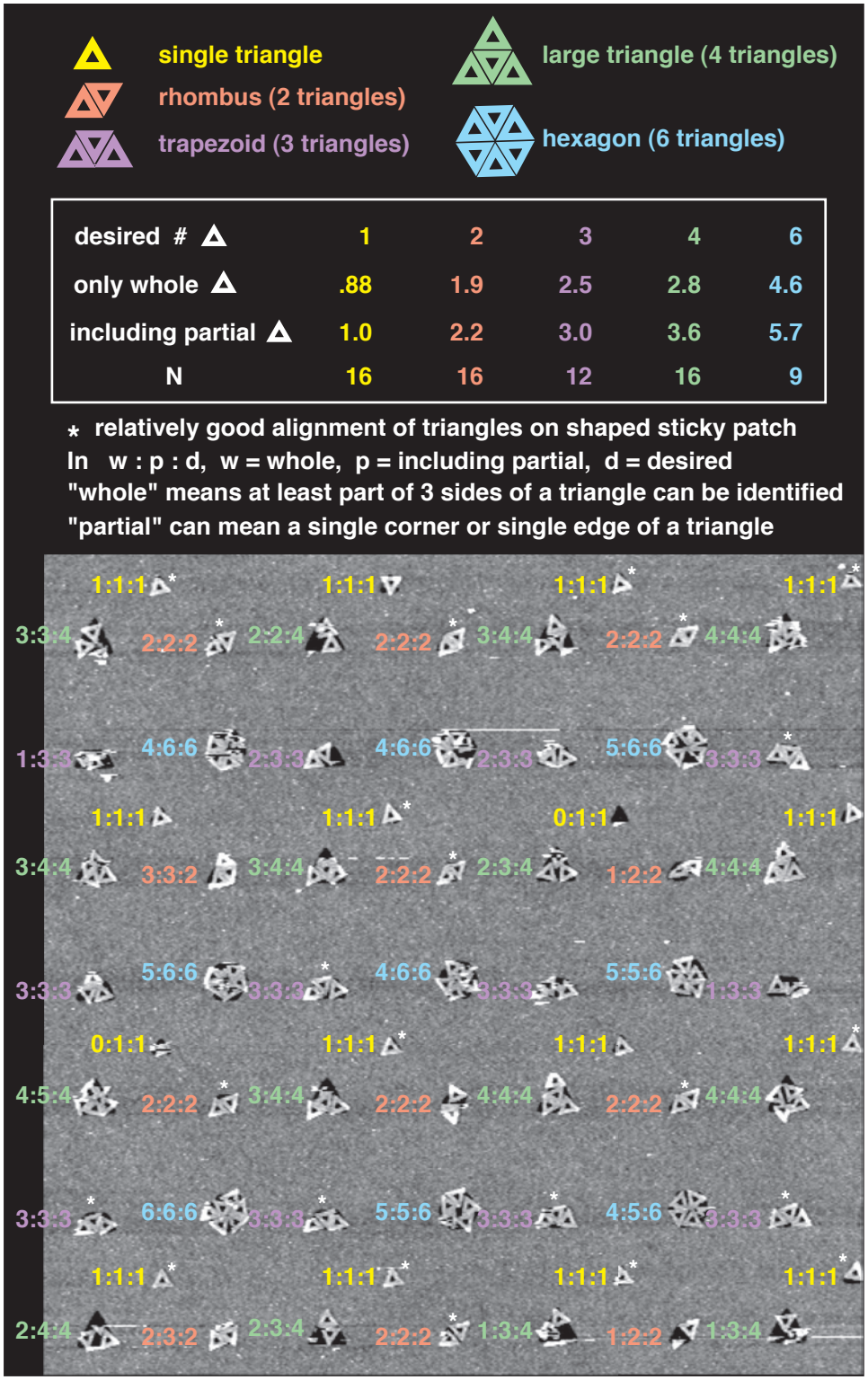

Figure S25: **Triangles on a DLC surface patterned with multiple shapes based on a ~121 nm unit-sized binding site.** Annotated 3 μm height image, with a table giving the average number of triangles bound to each shape. Partial triangles were counted if even a single corner or edge could be seen.

DOI: 10.1038/NNANO.2009.220

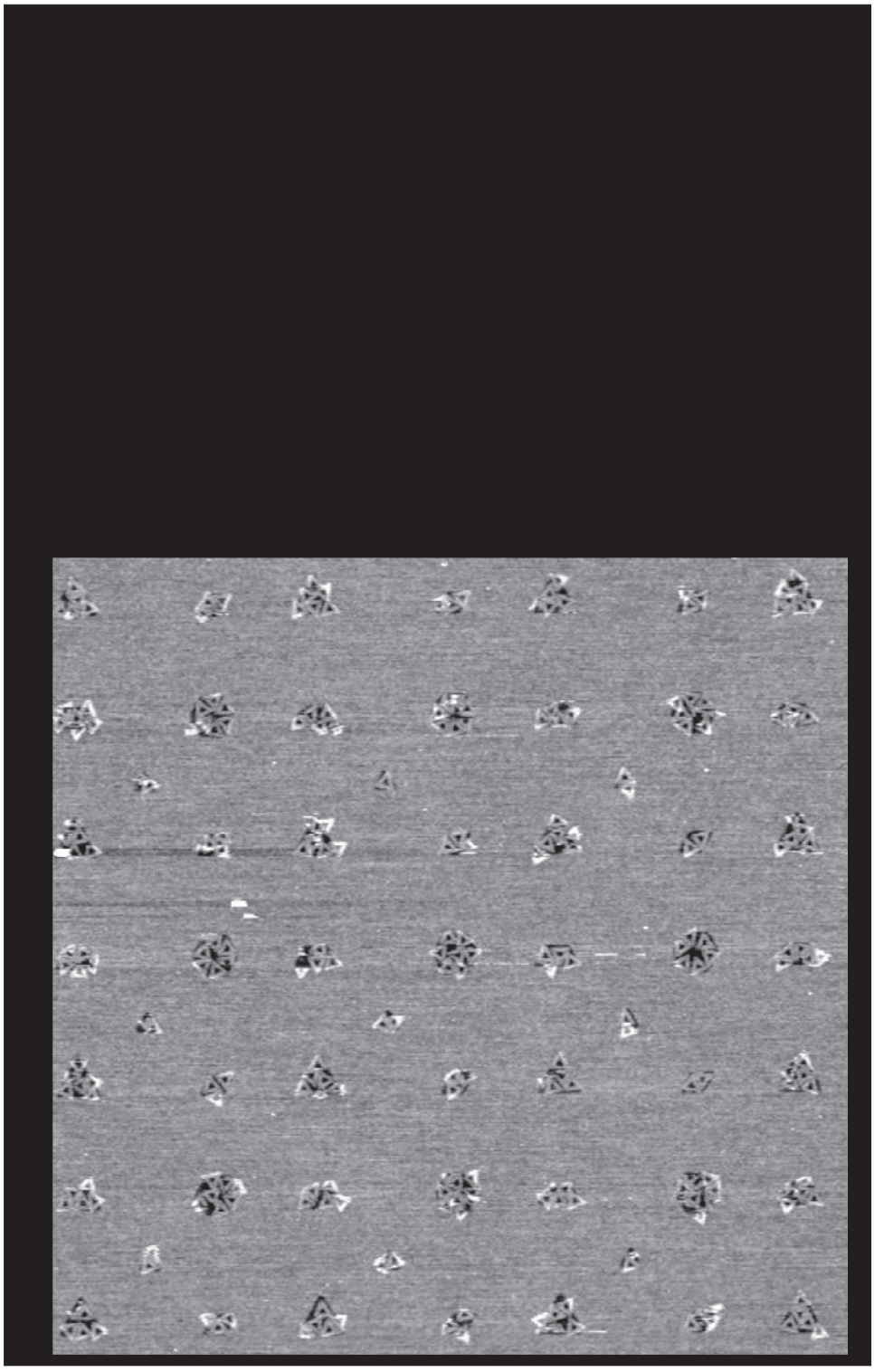

Figure S26: **Triangles on a DLC surface patterned with multiple shapes based on a ∼145 nm unit-sized binding site..** Unannotated 3 μm height image. Height scale is 3 nm, and runs from black (0 nm) to white (3 nm).

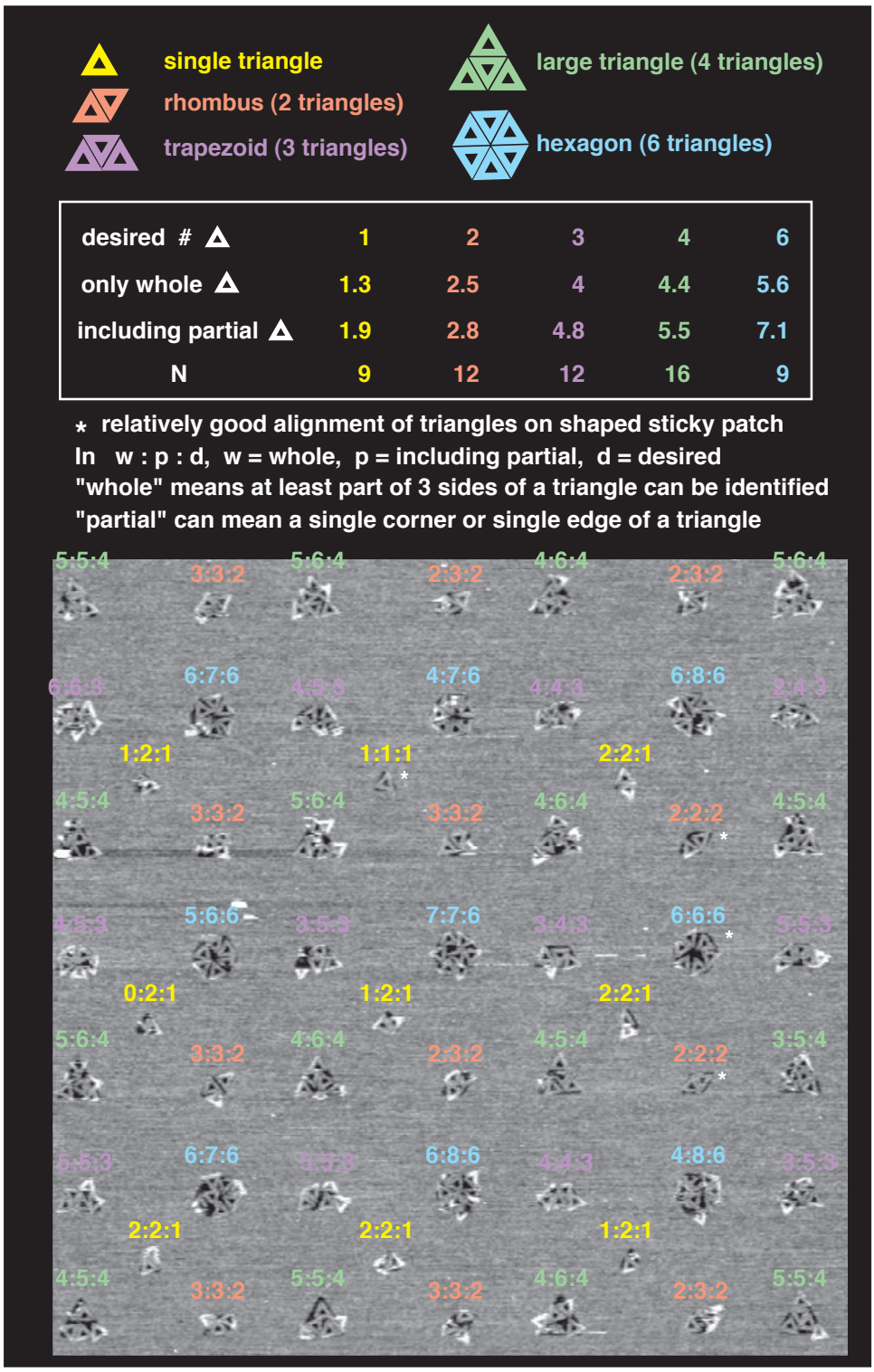

Figure S27: **Triangles on a DLC surface patterned with multiple shapes based on a ~145 nm unit-sized binding site.** Annotated 3 μm height image, with a table giving the average number of triangles bound to each shape. Partial triangles were counted if even a single corner or edge could be seen.

DOI: 10.1038/NNANO.2009.220

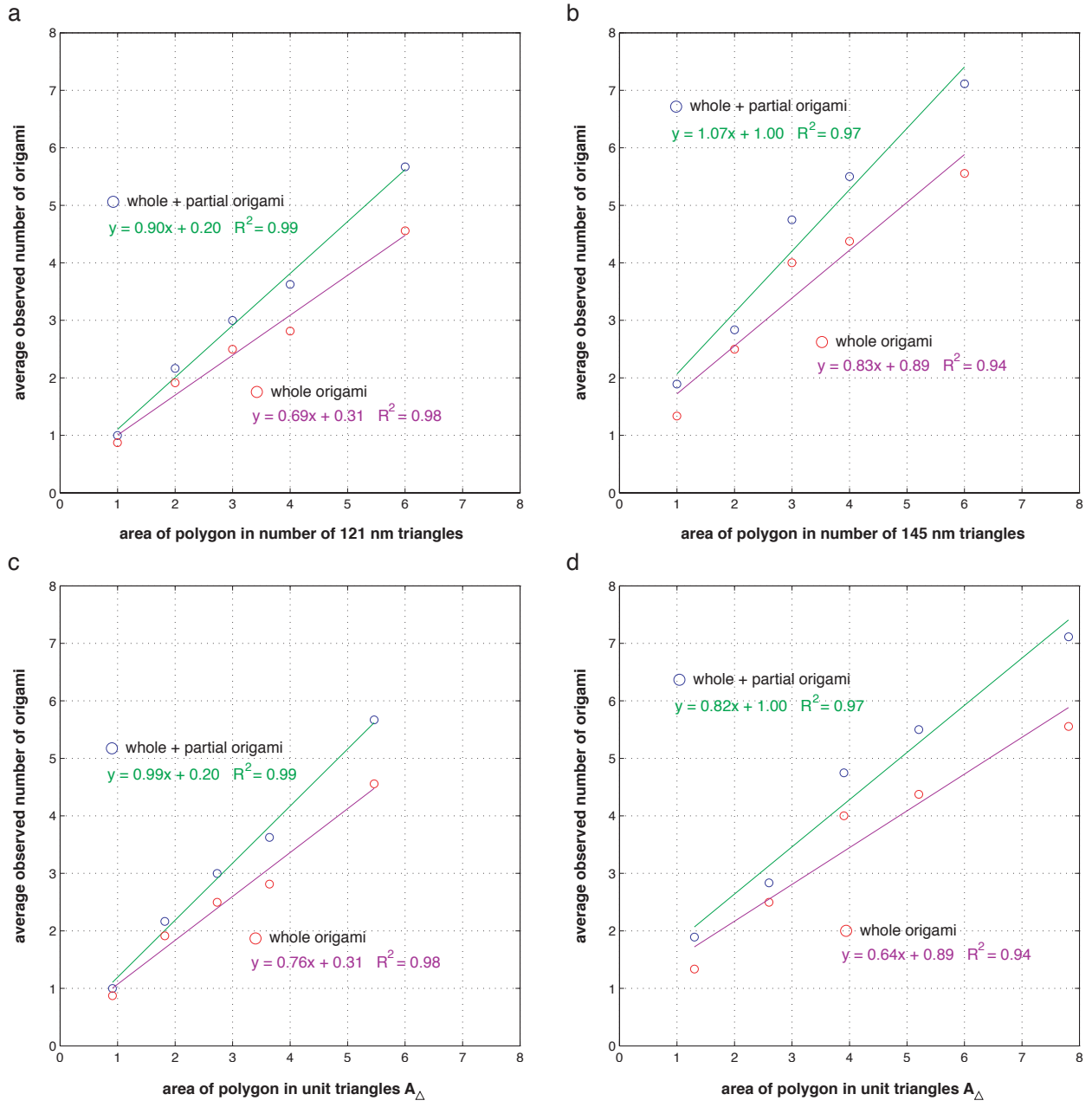

Figure S28: **Line fits to the data from Figs. S25 and S27.** DNA triangles were assumed to be 127 nm; sizes of sticky features were measured relative to the triangles. Fits to whole origami data (red circles) are given as purple lines. Fits to (whole + partial) origami data (blue circles) are given as green lines. (**a**) and (**c**) show data for Fig. S25 with features whose shapes are based on a triangle roughly 121 nm on side. (**b**) and (**d**) show data for Fig. S27 with features whose shapes are based on a triangle roughly 145 nm on side. In (**a**) and (**b**) the average number of bound origami is plotted against the area of the sticky features, expressed in terms of the area of the single triangle sticky patch, 121 or 145 nm; this is the number of origami that were intended to bind a given feature. In (**c**) and (**d**) the x-axis has been normalized so that the average number of bound origami is plotted against the area of the sticky features expressed in terms of the area of the DNA triangle.

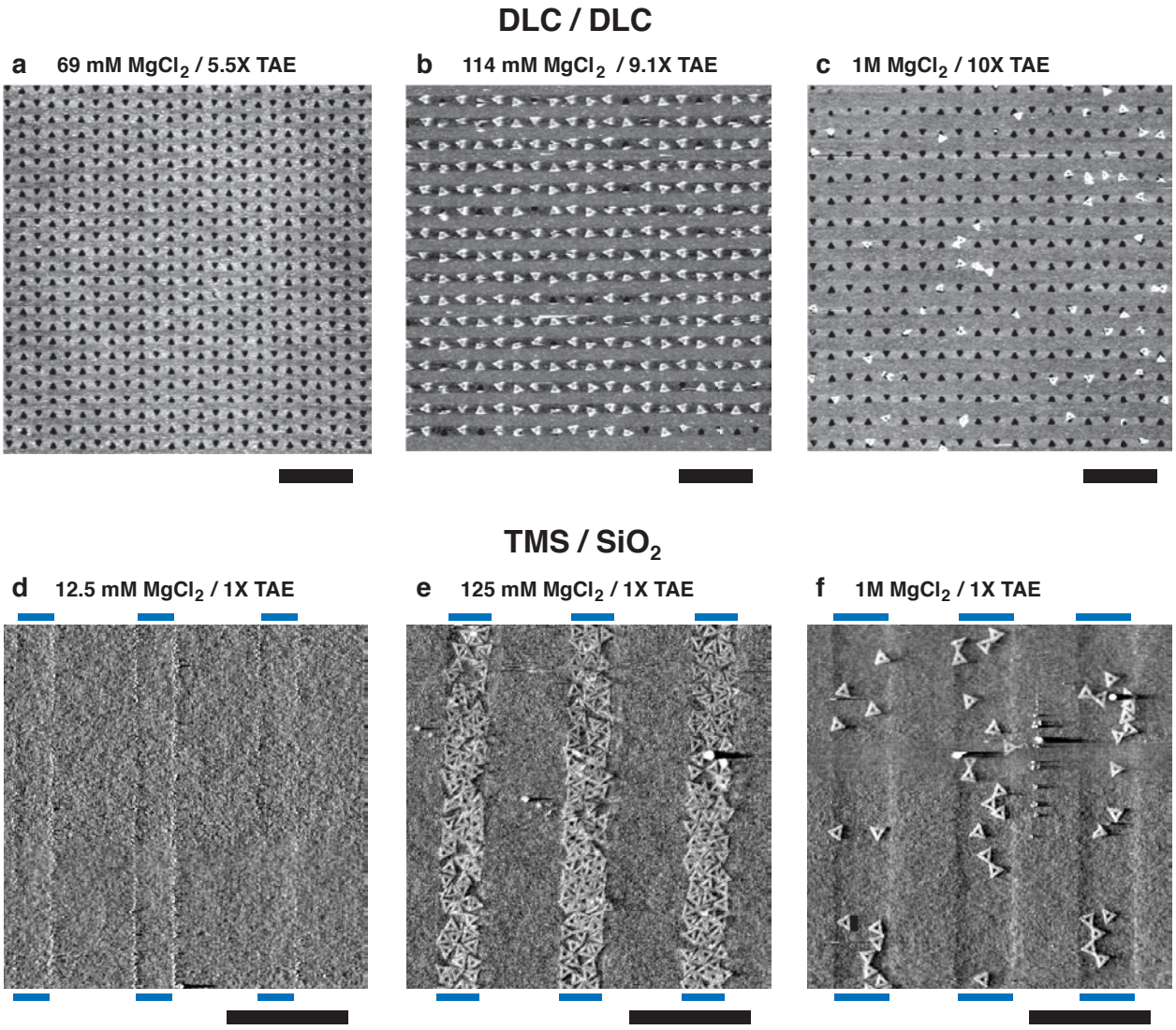

Figure S29: **Origami binding under various salt conditions.** (**a**)–(**c**) Binding on triangular features on DLC/DLC. On DLC/DLC binding is not observed using 12.5 mM $MgCl_2$/1X TAE (not shown) but is observed (**b**) with a solution that is ∼10X more concentrated for both components. Panel (**a**) conditions (∼5X both components) were explored in an attempt to find the salt concentrations at which origami begin to bind. Panel (**c**) shows that increasing the concentration of $MgCl_2$ to 1 M (with TAE fixed at 10X, comparable to **b**) greatly decreases binding efficiency and removes orientational selectivity. (**d**)–(**f**) Binding on optically-patterned line features (300 nm, 350 nm and 450 nm) on TMS/SiO_2 at fixed (1X) TAE concentration and increasing $MgCl_2$ concentration. Blue bars indicate width of sticky line features. (**d**) 12.5 mM $MgCl_2$ is not sufficient for binding. (**e**) high-density binding is observed at 125 mM $MgCl_2$. (**f**) poor binding at 1 M $MgCl_2$. All scale bars are 1 μm.

An atomic force micrograph (AFM) movie showing the dynamic binding of DNA origami to triangular features (of a variety of sizes) on a diamond-like carbon substrate. Single origami bind and align best to size-matched features. Some of the dynamics may be attributable to force exerted by the AFM tip.